UNIVERSITY OF TURKU

ELECTROSTATIC INSTRUMENTATION AND MEASUREMENTS ON POWDERS AND POWDER MIXTURES

Janne Peltonen

TURUN YLIOPISTON JULKAISUJA – ANNALES UNIVERSITATIS TURKUENSIS
SARJA - SER. AI OSA - TOM. 606 | ASTRONOMICA - CHEMICA - PHYSICA - MATHEMATICA | TURKU 2019

UNIVERSITY OF TURKU

ELECTROSTATIC INSTRUMENTATION AND MEASUREMENTS ON POWDERS AND POWDER MIXTURES

Janne Peltonen

TURUN YLIOPISTON JULKAISUJA – ANNALES UNIVERSITATIS TURKUENSIS
SARJA - SER. AI OSA - TOM. 606 | ASTRONOMICA - CHEMICA - PHYSICA – MATHEMATICA | TURKU 2019

University of Turku

Laboratory of Industrial Physics
Department of Physics and Astronomy
Faculty of Science and Engineering

Supervised by

PhD. Matti Murtomaa
Laboratory of Industrial Physics
Department of Physics and Astronomy
University of Turku
Turku, Finland

Reviewed by

Prof. Tatsushi Matsuyama
Department of Science and Engineering
for Sustainable Innovation
Soka University
Japan

PhD. Peter Ireland
School of Engineering
University of Newcastle
Australia

Opponent

Assoc. Prof. Maciej Noras
Engineering Technology and
Construction Management
University of North Carolina at Charlotte
United States of America

The originality of this publication has been checked in accordance with the University of Turku quality assurance system using the Turnitin OriginalityCheck service.

ISBN 978-951-29-7655-3 (PRINT)
ISBN 978-951-29-7656-0 (PDF)
ISSN 0082-7002 (Print)
ISSN 2343-3175 (Online)

Grano Oy - Turku, Finland 2019

Acknowledgements

This work has been carried out in Laboratory of Industrial Physics of the Department of Physics and Astronomy at University of Turku. I would like to thank the Doctoral Programme in Physical and Chemical Sciences (PCS) and the University of Turku Graduate School (UTUGS) for the funded doctoral candidate position in 2016–2019. PCS and Turun yliopistosäätiö are acknowledged for the travel grants.

The Laboratory of Industrial Physics has been an outstanding place to work. I cannot say enough positive words about the great atmosphere. The humour has been dry and coffee consumption huge. Most of all, I am grateful to my supervisor Dr. Matti Murtomaa. I became interested in electrostatics when I attended his course about the subject. I had thought that static electricity was just a phenomenon widely used in science demonstrations for kids. I also knew that it was the reason why I got electric shocks in winter. But I did not known that electrostatic charging had such a big impact on the pharmaceutical and electronics industry, and even the physicists did not understand it satisfactorily. And this man was studying it! In retrospect, I think it was inevitable that I would do my own PhD studies about electrostatics as well. Thank you, Matti, for your never-ending guidance, expertise and help. I never felt I was alone with the research but a part of a team. Thank you Prof. Jarno Salonen for being the head of the laboratory. Thank you for all your support and advice. I also thank the rest of the fellow Teofys-people in the past and today: Jorma, Ermei, Outi, Teija, Jaani, Luke, Jaakko, Rici, Martti, Maija, Antti, Tero, Martta, Sirja and Sanna-Mari.

I thank my opponent Assoc. Prof. Maciej Noras. Prof. Tatsushi Matsuyama and Dr. Peter Ireland are acknowledged for reviewing this thesis. I also thank my co-authors Dr. Kelly Robinson, Outi Alanen, Ermei Mäkilä and Aleksi Saikkonen. The Electrostatics Society of America, the friendly society, is acknowledged for organizing such student-friendly and pleasant conferences and accepting my abstracts for oral presentations. I always felt that my research was appreciated. Especially, thank you for organizing the 2017 meeting in Ottawa, Canada so I had to possibility to go to see the Canadian Grand Prix in Montreal before the conference! Staattisen sähkön hallinta STAHA yhdistys ry is acknowledged for the granted stipend at the end of my master's degree studies and for the interesting meetings that broadened my knowledge on industrial processes involving static electricity.

A big thanks to all of my friends. Especially I thank my fellow physics students Henri, Janne and Samuli. I never would have graduated without such team spirit and

legendary moments as a student, usually not related to studying at all. Tee tiärätte.

I am deeply grateful to my parents Taina and Pentti for the safe childhood and for making this journey possible. There's no place like home. Thank you Ville, Essi and little Alvin. Thank you Heidi and Henri. Thank you Mummi and all other relatives. Kiitos Matti-setä. Finally, I thank my dearest Outi for all the moments together. You are the best.

Turku, April 2019

Janne Peltonen

Abstract

In the powder industry, such as the pharmaceutical or chemical industry, powder particles collide frequently with the surrounding surfaces and with other particles and become electrostatically charged in different processes. The charging may cause problems, for example, in powder mixing and conveying. High charge values increase particle adhesion on surfaces. Charged particles may adhere to sensors or production lines of a pharmaceutical plant. In the worst case, even a dust explosion may occur.

The aim of this work was to develop instrumentation for these kinds of processes and to study the charging and electrical resistivity of powders and powder mixtures. The charge and resistivity are the fundamental quantities when electrostatic effects are studied. The charge is a direct measure for the intensity of the electrostatic charging, and the resistivity is related to the dissipation of the accumulated charge.

In the thesis, a method for studying the powder resistivity as a function of humidity was developed. The new method proved to be significantly faster than the traditional steady-state measurements. For instance, the resistivity of a lactose powder was measured in 24 hours with the new one-step method but took four weeks with the traditional method. The electrical resistivity of powder mixtures was also studied. It was observed that the particle size difference of the component materials played an important role in the effective resistivity.

Two induction probes for measuring the charge density of powder in a fluidized bed were developed. The probes were designed using computer simulations, calibrated with frictionally charged spheres, and finally tested in a laboratory-scale fluidized bed.

The charging of lactose and salbutamol sulphate was studied at different humidities. The humidity had a special effect on the charging of their mixtures. At low humidities, the mixtures charged negatively. As the humidity was increased, the charge polarity flipped from negative to positive. When the once humidified samples were dried, the polarity did not flip back to negative but remained positive. It was suggested that the small salbutamol sulphate particles adhered to larger lactose particles due to increased capillary forces and remained adhered even if the powder was again dried.

A method for studying the charging of powders on-line during surface adhesion was also developed and used in measurements. The powder was slid in a pipe, and the charge and mass of the transferred powder were simultaneously monitored. With powder mixtures, it was observed that the dominant charging mechanism changed from powder–pipe contacts to powder–powder contacts between the two dissimilar powders quickly after the other powder component started to adhere to the pipe surface.

Tiivistelmä

Teollisissa prosesseissa, joissa käsitellään toisiaan vasten hankautuvia eristäviä jauheita, esiintyy lähes aina merkittävässä määrin sähköistä varautumista. Sähköinen varautuminen taas aiheuttaa prosessiongelmia esimerkiksi jauheiden kuljetuksessa, sekoituksessa ja pakkaamisessa. Jauhepartikkelit tarttuvat voimakkaasti tuotantolinjaston pintoihin suuren varauksen takia, minkä takia tuotanto voidaan joutua toistuvasti keskeyttämään puhdistusta varten. Pahimmassa tapauksessa sähköinen läpilyönti saattaa aiheuttaa räjähdyksen pölyisässä ja herkästi syttyvässä ympäristössä.

Tämän tutkielman tarkoitus oli kehittää mittausmenetelmiä ja tehdä mittauksia jauheiden ja jauheseosten sähköstaattisten ominaisuuksien tutkimiseksi. Tärkeimmät tutkitut suureet olivat varaus ja sähköinen resistiivisyys. Varaus kuvaa suoraan varautumisen suuruutta, ja resistiivisyys kertyneen varauksen poistumisnopeutta.

Tutkielmassa kehitettiin uusi menetelmä jauheen resistiivisyyden kosteusriippuvuuden tutkimiseksi. Uusi menetelmä osoittautui perinteistä menetelmää huomattavasti nopeammaksi. Lisäksi havaittiin, että jauheseosten resistiivisyyteen vaikuttavat huomattavasti seosmateriaalien resistiivisyys ja partikkelikokoero.

Tutkielmassa kehitettiin kaksi mitta-anturia jauheen varaustiheyden reaaliaikaiseksi mittaamiseksi leijupetireaktorissa. Anturit suunniteltiin tietokonesimulaatioilla, kalibroitiin kokeellisesti varatuilla palloilla ja lopulta käytettiin mittauksissa leijupetisysteemissä.

Lisäksi tutkittiin kosteuden vaikutusta laktoosin ja salbutamolisulfaatin varautumiseen. Kosteuden lisäämisellä oli erikoinen vaikutus seosten varautumiseen. Pienissä kosteuksissa seokset varautuivat negatiivisesti, mutta varauksen merkki vaihtui positiiviseksi kosteuden kasvaessa ja pysyi positiivisena kuivauksesta huolimatta. Oletettavasti salbutamolisulfaattipartikkelit tarttuivat laktoosipartikkeleihin kasvaneiden kapillaarivoimien vaikutuksesta eivätkä irronneet kuivauksessa.

Lopuksi kehitettiin reaaliaikainen varautumismittausmenetelmä adheesion vaikutuksen tutkimiseksi. Jauhe varattiin liu'uttamalla putkessa. Putkesta ulos liukuneen jauheen varaus ja massa määritettiin samanaikaisesti. Jauheseoksilla havaittiin, että aluksi kontaktit jauhepartikkelien ja putken kanssa hallitsivat varautumista. Kun toinen seoskomponentti alkoi tarttua putken pintaan, kontaktit jauhekomponenttien välillä alkoivat hallita varautumista.

List of Publications

This thesis is based on experimental work carried out in the Laboratory of Industrial Physics, Department of Physics and Astronomy, University of Turku during the years 2015–2018. The thesis consists of an introductory part and of the following publications:

[I] M. Murtomaa, J. Peltonen and J. Salonen: *One-step measurements of powder resistivity as a function of relative humidity and its effect on charging*, Journal of Electrostatics **76**, 78–82 (2015).

[II] J. Peltonen, M. Murtomaa and J. Salonen: *A coaxial induction probe for measuring the charge, size and distance of a passing object*, Journal of Electrostatics **77**, 94–100 (2015).

[III] J. Peltonen, M. Murtomaa, A. Saikkonen and J. Salonen: *A coaxial probe with a vertically split outer sensor for charge and dimensional measurement of a passing object*, Sensors and Actuators A: Physical **244**, 44–49 (2016).

[IV] J. Peltonen, O. Alanen, E. Mäkilä, M. Murtomaa and J. Salonen: *Influence of relative humidity on the electrostatic charging of lactose powder mixed with salbutamol sulphate*, Journal of Electrostatics **88**, 201–206 (2017).

[V] J. Peltonen, M. Murtomaa, K. Robinson and J. Salonen: *The electrical resistivity and relative permittivity of binary powder mixtures*, Powder Technology **325**, 228–233 (2018).

[VI] J. Peltonen, M. Murtomaa and J. Salonen: *Measuring electrostatic charging of powders on-line during surface adhesion*, Journal of Electrostatics **93**, 53–57 (2018).

Contents

1. Introduction

Modern physics can describe the very first seconds of the universe. It can describe how heavy elements in our bodies and in our surroundings have been formed through nuclear fusion inside stars. Yet modern physics cannot satisfactorily explain why a balloon becomes electrostatically charged when it is rubbed against a piece of fabric.

Even though electrostatic charging (*i.e.* triboelectric charging, triboelectrification) is a well-known phenomenon, it is surprisingly poorly understood. When two surfaces of different materials are brought into contact, electric charge is able to move from one surface to the other. When the surfaces are separated, some of the charge is not able to flow back to the original surface. As a result, the surfaces have become electrostatically charged, one positively and the other negatively. However, even modern physics cannot predict which of the surfaces charges positively, which negatively and how much charge is transferred. In fact, there is no consensus on whether the charge carriers are electrons, ions or tiny pieces of material.

Electrification has a tremendous effect in nature. For instance, a lighting bolt is a consequence of triboelectric charging in clouds. In industrial processes, electrostatic charging is often regarded as an inconvenience. Electrostatic discharges are a major problem in the electronics industry where components have become smaller and more compact. In the powder industry, small powder particles impact frequently with each other and with surfaces nearby and become charged. The charging may cause problems, for instance, in powder mixing and conveying. High charge values increase particle adhesion on surfaces. Charged particles may adhere to sensors, production lines of a pharmaceutical plant or solar panels in a distant desert. In the worst case, powder dust may explode if a discharge occurs. However, despite such complications, electrostatics has also numerous useful applications. For example, digital printing and xerography are based on precise controlling of charged toner particles.

Experiments must be performed and new instrumentation techniques must be developed in order to understand and control static electricity. In this thesis, triboelectric

charging and electrical resistivities of powders and powder mixtures are studied, and the current understanding of charging and its impact on selected industrial processes are reviewed. After a brief introduction in chapter 1, electrostatic charging as a phenomenon is discussed in chapter 2. Next, in chapter 3, some measurements methods relevant to this thesis are presented. The effect of charging on selected industrial branches is briefly discussed in chapter 4. Chapter 5 introduces the objectives of the thesis. The used materials and methods are presented in chapter 6 and the results in chapter 7. The conclusions are given in chapter 8.

2. Electrostatic charging

2.1 Contact charging and triboelectric charging

When two initially neutral materials are brought into physical contact with each other, charge separation can occur so that the surface of one material gains a positive and the other a negative electric charge. If at least one of the materials is insulating, the charge separation will remain if the materials are separated (Fig. 2.1). If the materials are rubbed together during the contact, they are said to become electrostatically charged by triboelectric charging or triboelectrification. Often the terms ”contact charging” and ”triboelectric charging” are considered interchangeable since completely frictionless contacts are difficult to produce. In addition, it is well-known that rubbing increases

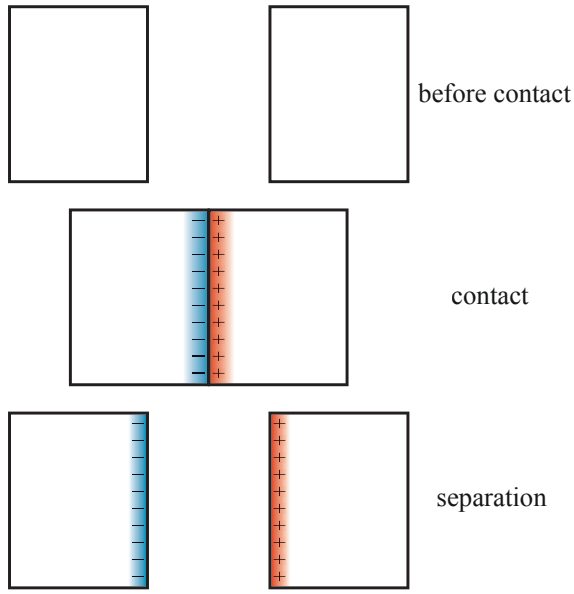

Figure 2.1: A simple illustration of contact charging.

Table 2.1: An example of a triboelectric series [10]. A material closer to the top of the series becomes positively charged as it is brought into a contact with a material lower in the series.

+	Glass
	Nylon
	Wool
	Cotton
	Steel
	Wood
	Amber
	Copper
	Silver
	Gold
	Polyester (PES)
	Polyethylene (PE)
	Polypropylene (PP)
	Polyvinyl chloride (PVC)
–	Teflon (PTFE)

charging but the reason is not completely understood [1].

Even though the phenomenon of electrostatic charging is observed in many everyday situations, the physical theory behind it is poorly understood. In fact, it is not even known with certainty whether the charge carriers are electrons, ions [2, 3], very small pieces of the materials [4–7], or a combination of all of these [8]. Over the years, the published literature has mainly concentrated on electron transfer theory, but interesting studies on ion and material transfer have also been published.

The physics behind charging is very complex. It is estimated that on a highly charged surface there are only a few extra charge carriers (or a deficiency of them) per one million atoms [9]. Thus, computer simulations are very time consuming, and experiments are hard to reproduce since small variations in surface conditions, experimental conditions (humidity etc.) and the nature of the contact will have significant consequences on charging behaviour [8]. The situation is further complicated by the fact that charged surfaces are in non-equilibrium states [1].

Generally, it is impossible to predict the magnitude or even the sign of the charge when two materials are brought into contact [11]. A triboelectric series is an empirical list where materials are arranged based on the sign of the charge that they gain when

they are in contact with other materials in the series. Materials that are higher in the series gain a positive charge when in contact with a material lower in the series. However, different studies often result in different orderings, and the results are difficult to reproduce. In addition, some materials cannot be arranged into a series. An example of a triboelectric series is presented in Table 2.1 [10].

In most cases the charge is not uniformly distributed on the surfaces, but rather as ”mosaic” of small oppositely charged regions resulting in a net charge of one polarity [12].

2.2 Electron transfer

2.2.1 Electron energies in materials

In isolated atoms, the electrons are quantized on certain discrete energy states. As materials are formed from several atoms, the energy states broaden and become less accurately defined. The energy ranges become virtually continuous, and are known as energy bands. The highest occupied energy is the Fermi energy, and the energy that is required to move an electron from the Fermi energy level to infinity is called work function. The energy range that is empty of possible energy states is known as a band or energy gap. A charge carrier cannot have an energy state that is in the band gap. The most important bands and band gaps are the ones whose energies are close to the Fermi level. The energy band above the band gap, where electrons can be excited, is called the conduction band. The band below the band gap is called the valence band. The electrons in the conduction band are responsible for the electrical conductivity of the material [13].

A material is conductive, semiconductive, or insulating depending on energy bands structure [14]. This is illustrated in Fig. 2.2. In a conductor, the conduction and valence band overlap, *i.e.* there is no energy gap between the bands. As a result, the conductivity is high since there is a large amount of free charge carriers. A conductive system is also achieved if the bands are only partially occupied [13, 15]. With semiconductors and insulators, there is an energy gap between the conduction and valence band. The valence band is fully occupied with electrons and the conduction band is completely unoccupied.

In reality, perfect insulators do not exist. Real-life insulators conduct electricity slightly due to additional energy states caused by the impurities, crystal defects, and the so called surface states that are formed when the symmetry of the bulk material is

broken on the surface. The additional energy states may be located in the energy gap. Electrons may be able to be thermally excited from these states and can thus act as charge carriers.

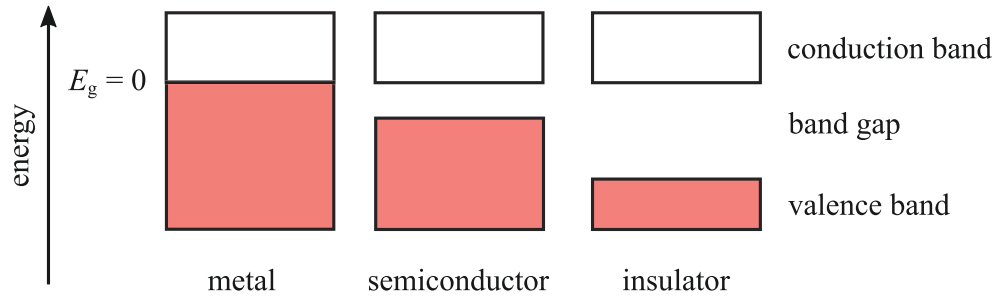

Figure 2.2: A schematic illustration of energy bands and band gaps for metal, semiconductor, and insulator. The horizontal axis has no physical meaning in this illustration.

2.2.2 Metal–metal contact

Charging in a metal–metal contact is well understood [16]. If two metals with different work functions are brought into contact, there is a contact potential difference V_c between the metals and the electrons are able to minimize their energy by moving from the metal with the lower work function (W_1) to the metal with the higher work function (W_2). The contact potential difference V_c can be calculated from the work functions as

$$V_c = -\frac{W_1 - W_2}{e}, \tag{2.1}$$

where e is the elementary charge. With metals, the work function is usually from 3 eV to 5 eV. The charge separation creates an electric field opposite to the initial potential difference and sets a limit for the charge flow. Eventually, the Fermi levels of the metals are lined up (Fig. 2.3), and as a result, the metal with the larger work function is charged negative and the one with the lower work function is charged positive. The amount of transferred charge can be calculated as the product of the contact potential difference and the capacitance between the contacting metals. The transferred charge is able to move away from the contact point due to the high conductivity of metals. Therefore, the charging of metals is usually unnoticeable. However, if the metals are insulated after the contact, the charge can be measured [17]. The aforementioned model suggests that the transferred charge depends linearly on the contact potential difference. Results reported by Harper [18] had the same linear tendency as the model proposes, even though

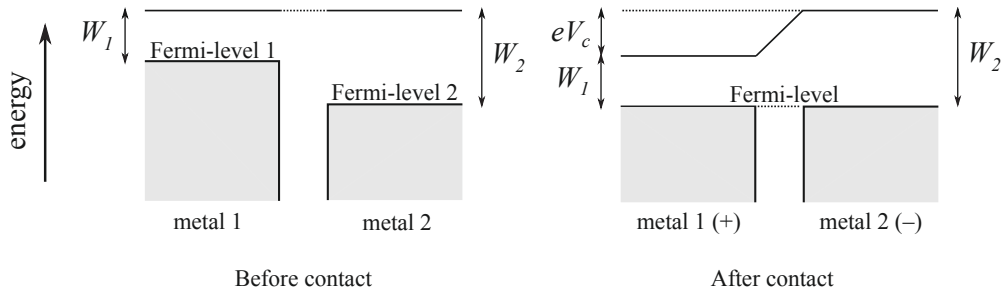

Figure 2.3: When two metals come into contact, their Fermi levels line up.

the experimental values were consistently smaller (Fig. 2.4). Harper suggested that this was due to imperfections, such as oxide layers, on the contacting surfaces. The experimentally observed linearity implies that electrons are the major charge carriers that are transferred in a metal–metal contact. However, some of the transferred charge may probably be able to flow back to the original surface as the surfaces are being separated.

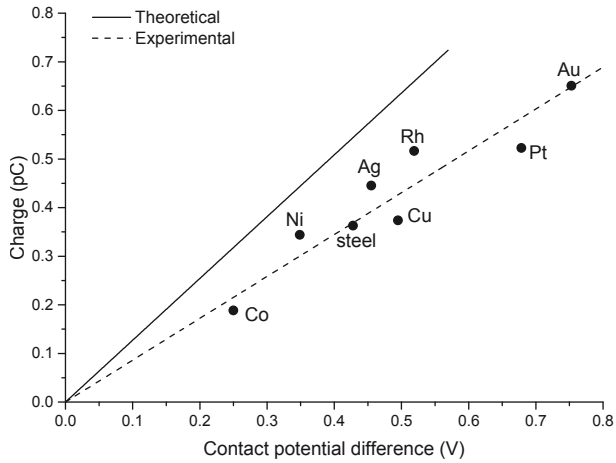

Figure 2.4: Charge accumulated on a chromium sphere (diameter 4 mm) in a contact with another metal spheres (diameter 13 mm) as a function of the contact potential difference. Adapted from [17], data from [18].

2.2.3 Insulator–metal contact

The conduction band of a perfect insulator is completely unoccupied, the valence band is completely occupied, and the bands are separated by a large band gap. Moreover,

the energy states of electrons in the valence band of an insulator are not as well defined as they are in conductors. Thus, the concept of work function is not valid for insulators. Instead, an effective or apparent work function, similar to the work function with metals, is often assigned for insulators; the basic idea is that electrons will move in a contact to a lower energy state from one surface to the other. Some experimental studies have shown that in a non-sliding insulator–metal contact, the amount of the transferred charge is proportional to the work function of the contacting metal [19, 20]. From the measured data, the effective work function can be defined to be the contact potential value at the zero charge intercept [8]. However, the data is often widely scattered and contradicting results have also been obtained when repeated contacts in a same position have been performed [13, 21, 22]. Moreover, a problem with the effective work function is that there are no free electrons available in insulators, thus, other models have to be presented.

2.2.4 Insulator–insulator contact

The charge transfer in an insulator–insulator contact is poorly understood, and many theoretical models have been presented over the years [23]. As discussed earlier, the problem with the effective work function is that there are no free electrons in insulators. To explain charging in an insulator–insulator contact, other models have been proposed; the surface state model assumes that the available electron energy states, responsible for the electrostatic charging, are located only on the surface of the insulator [23]. When two insulators are brought into contact, electrons move from the filled surface states of the first insulator to the empty surface states of the other insulator. Again, the direction of the charge transfer is determined by the contact potential difference of the surfaces so that the electron will be at a lower energy state after the transfer.

As discussed earlier, additional energy states are formed into the band gap also due to crystal defects and impurities. Also, the imperfection of the surface (such as oxide layers, adsorbed molecules, surface roughness etc.) plays an important role in insulator charging.

2.3 Ion transfer

There is evidence that in situations where mobile ions are present in insulating materials, the electrostatic charging is caused by transferred ions instead of electrons [24–26]. In some materials, there are tightly bound ions with one charge polarity on the surface

and oppositely charged ions loosely bound to these ions. When this kind of a material comes to contact with another material, the loosely bound ions may be transferred. The contact material becomes charged with the polarity of the loosely bound ions whereas the original material has the polarity of the tightly bound ions [1]. Ion transfer has been proposed as the cause of charging also for materials that do not inherently have mobile ions on their surfaces. It is suggested, for example, that OH^- ions in the water layer adsorbed onto the surface are transferred when two materials are brought into contact [27].

2.4 Material transfer

Charging by material transfer has been observed with polymers [6]. Especially in frictional contacts, small patches of material transfer from one surface to the other. Material transfer has been verified with X-ray photoelectron spectroscopy and Raman spectroscopy [12, 28]. Since chemical bonds must be broken for material to transfer, the transferred material is likely to transfer charge [1]. An extensive survey on material transfer is included, for example, in the review by Galembeck et.al. [7].

2.5 Charging of single particles

Electrostatic charging plays a significant role in various industrial processes where powders are handled, for instance in the pharmaceutical industry [29–32]. Powder particles collide with each other and with the walls of the system and gain an electrostatic charge. The electric force on small particles can be higher than the gravitational forces, causing small particles to adhere to the walls. In order to understand the charging behaviour of powders, it is important first to understand the charging of single particles.

A simple resistor–capacitor analogy can be used as a model for the charge transfer between an interface between two materials (Fig. 2.5) [33, 34]. If a particle is on a conducting plane, the accumulation of charge on its surface is analogous to the charging of a capacitor. The driving force for the charge transfer is the contact potential difference V_c caused by the difference in the work functions (or effective work functions). This is countered by the voltage V_acc caused by the image charge that is found on the conducting surface. If it is assumed that the resistance R of the charging path obeys Ohm's law, the charging rate is given by the equation

$$\frac{\mathrm{d}q}{\mathrm{d}t} = \frac{V_\mathrm{c} - V_\mathrm{acc}}{R}, \tag{2.2}$$

where t is the contact time. If the contact area is S and surface charge density σ, the capacitance of the system is given by $C = \sigma S/V_{\text{acc}}$. The charge transfer stops when the voltage V_{acc} totally counters the driving voltage V_c. This is analogous to a fully charged capacitor.

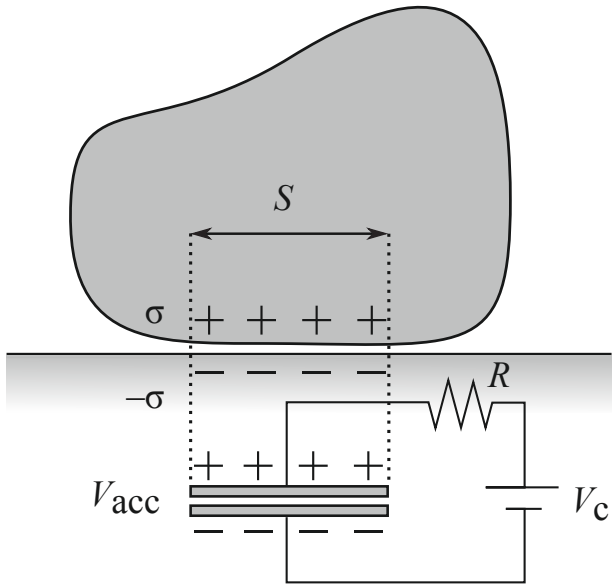

Figure 2.5: The capacitor analogue of contact charging between a particle and a conductive plane. Adapted from [33] and [35].

When an individual particle hits a metal plate, its charge after the collision depends on its initial charge and on the impact velocity. The charge that is transferred during the impact (Δq) is the difference between the final (q_f) and initial charge (q_i) of the particle: $\Delta q = q_f - q_i$. This impact charge depends linearly on the initial charge. As the initial charge increases, an equilibrium value (q_e) where no charge is transferred is reached. A characteristic charge value (Δq_0) is observed when the initial charge is zero. The charge that is transferred in the impact can be expressed as

$$\Delta q = \Delta q_0 \left(1 - \frac{q_i}{q_e}\right). \tag{2.3}$$

An increase in the impact velocity increases the characteristic charge, while the equilibrium charge is unaffected [17, 36, 37]. The impact charging is also influenced by the impact angle [38, 39].

Studies show variation in the transferred charge as the number of contacts increases [40, 41], until a saturation value is achieved [42–45]. The saturation charge tends

to decrease as the time interval between subsequent impacts increases since the leakage of the accumulated charge increases with time. Chowdhury et.al. [46] showed that the saturation charge for polyethylene particles in contact with a metal was directly proportional to the surface area of the particles, a great indication that electrostatic charging is a surface phenomenon. On the other hand, Homewood et.al. studied charging of polyethylene and polytetrafluoroethylene in carefully controlled contacts with mercury and found that the charge did not vary when the contacts were repeated [47]. For a deeper understanding of mathematical analysis of repeated impacts, studies by Matsusaka et.al. [17, 44, 48] and Greason [43] are recommended.

2.6 Charging of powder flows

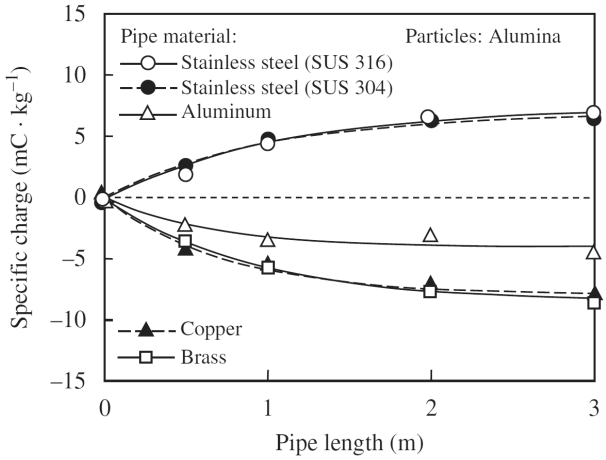

Figure 2.6: The charging of alumina particles as a function of the pipe length in gas–solid particle flow. Reprinted from [49] with permission from Elsevier.

With powders, the charging process becomes more complicated than with single particles since powder particles collide with each other and with the surrounding surfaces. The charging of powders is affected by numerous parameters (in addition to the material related properties), such as the geometry of the system, particle size distribution, mixture concentration [50], contamination of the contacting surfaces [51], etc. In powder flows, the behaviour of the flow plays an important role. In a simple case, the particles are sliding on a surface, but as the type of the contact changes from sliding to rolling or bouncing, the charging becomes more difficult to analyse [33, 34]. The

charge $Q(z)$ of a powder flow with a flow distance of z can be expressed as

$$Q(z) = Q_\infty \left[1 - \exp\left(-\frac{z}{z_\mathrm{c}}\right)\right], \tag{2.4}$$

where Q_∞ is the charge for an infinite long flow distance (*i.e.* saturation charge) and z_c a characteristic length in the charging process [52]. Experimental charging results in different pipe materials, reported by Matsusaka et.al. [49], are presented in Fig. 2.6.

In powder mixture flows, the charge of the transported powder is usually bipolar so that the sign is different for each powder species due to particle–particle contacts between the dissimilar materials [50, 53]. The oppositely charged particles can be separated using an electric field [54, 55]. If the mass of the particle is small, a high charge density may cause the powders to adhere to the surface. The charging profile may considerably change during the flow due to adhesion [50, 56]. With certain mixture concentrations, a neutral net charge may be observed: the individual particles may be highly charged but the electric field may be close to zero if observed at a distance. This may be favourable in most of the cases.

2.7 Charging of identical solids

One might expect that triboelectrification occurs only when two chemically different surfaces are in contact with each other. However, triboelectrification occurs also when the chemical compositions of the surfaces are the same [57]. Moreover, one might expect that in case of two chemically similar surfaces, the charge polarities would be random. However, Shaw and Hanstock [58] observed that when identical rods were rubbed together as one would bow a violin string, the rods charged in a systematic way. The polarities were reversed if the roles of the rods were reversed (the 'bow' become the 'string') [59, 60]. It has also been observed that in granular systems with a broad particle size distribution, the larger particles tend to charge positive and the smaller ones negative [61–73].

Several models have been proposed to explain these observations. Shaw and Hanstock [58] suggested that the systematic charging of rods of same material was caused by an asymmetry in the surface strains. Lowell and Truscott [59, 60] agreed that the strain plays a role in the charging but questioned if it is the actual cause of the charge transfer. The bipolar charging of granular systems, which was due solely to particle–particle contacts, was measured, simulated and mathematically explained by Lacks et.al. [71, 72, 74–78], based on studies by Lowell and Truscott [59, 60]. Their model

assumes that the charge carriers (electrons or ions) that are trapped into high-energy surface states are responsible for the charging process. Due to the insulating nature of the material, the charges at high-energy states cannot relax into lower energy states. A contact with another surface brings a high-energy state of a particle close to a another particle with a low-energy state, and thus enables the charge carrier to lower its energy by transferring from one surface to the other. The density of the occupied high-energy states and unoccupied low-energy states are assumed to be initially the same for the particles of different sizes. Thus, the absolute amount of surface energy states is larger for the larger particle since its surface area is larger. When the particles collide, there is a possibility for a charge in a high-energy state of one particle to transfer to a low-energy state of the other particle. In the first collision, it is equally probable that the

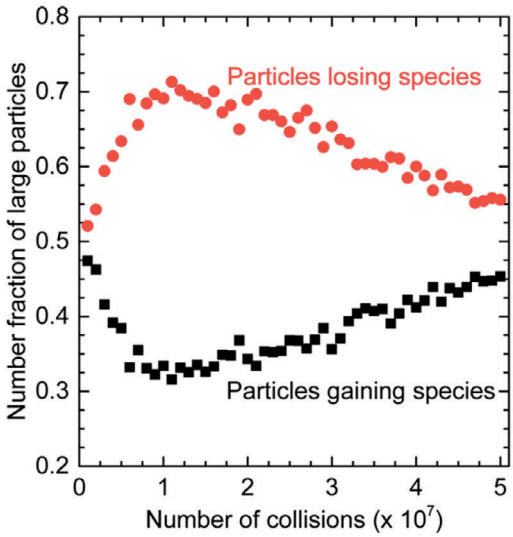

Figure 2.7: Monte-Carlo simulation results for number fraction of large particles that lost charge carriers or gained charge carriers. Reprinted with permission from [72]. Copyright 2017 American Chemical Society.

transferring charge originates from either particle. Therefore, it can be assumed that an equal amount of charge is transferred from a smaller to a larger as from a larger to a smaller particle when the particles first collide. However, after the first collision, the situation has changed in a significant way. The densities of the states are no longer equal for the two particles. Relatively higher amounts of high-energy states have now been unoccupied for the smaller particle, and therefore the density of occupied high-energy states is higher for the larger particle. As a result, for subsequent collisions, it is now

more probable for a charge to transfer from the larger particle to the smaller particle than in the opposite direction. The charges are systematically transferred to the smaller particle and, if it is assumed that the charges are electrons, they will become charged negatively while larger particles charge positively. A recent Monte-Carlo simulation by Toth et.al. [72] is presented in Fig. 2.7.

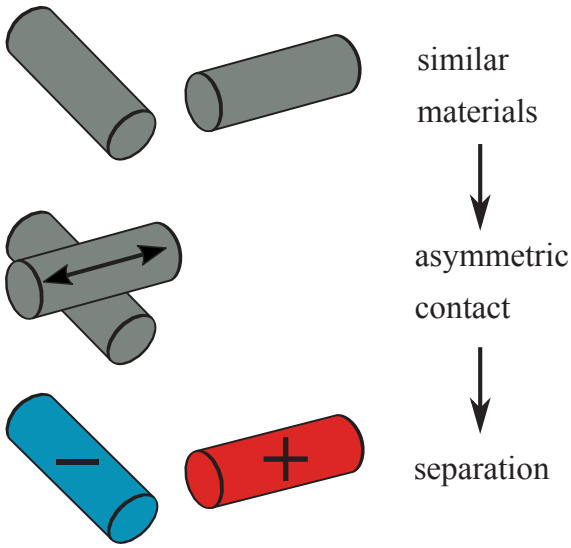

Figure 2.8: In an asymmetric contact between two similar materials, the charge carriers usually tend to accumulate on the body with the smaller contact area. In the picture, the stationary rod on the left has a smaller contact area compared to the rubbing rod. Therefore, if the charge carriers are electrons, the smaller contact area becomes negatively charged.

There are two mechanisms limiting the maximum amount of accumulated charge. First, the increasing electric field between the oppositely charged particles eventually prevents further charge transfer. Second, all the low-energy states become occupied or the high-energy states become unoccupied, and thus there are no more transferring charges available. Castle and Schein have shown that the electric field is the main mechanism limiting the charging [79]. Lowell and Truscott originally considered the charge species as electrons, but it has been pointed out that the model should be valid for ions as well [80, 81].

The aforementioned model is also valid for similar surfaces with an asymmetric contact: the charge carriers tend to accumulate on the surface with the smaller contact area while the larger surface area becomes depleted of them (Fig. 2.8). Pham et.al. [80]

studied contact charging between a rotating and a stationary cylinder of identical material. The stationary cylinder was contacted only at one point, while the rotating cylinder along its entire circumference. The rotating cylinder charged positively in teflon–teflon contacts, but negatively in nylon–nylon contacts. They suggested that the transferred charge carriers were negative in a teflon–teflon contact (perhaps electrons) but positive in a nylon–nylon contact (positive ions).

2.8 Induction charging

Induction charging occurs without an actual contact between the surfaces. If a neutral, conductive rod is brought into the vicinity of a positively charged sphere, the electrons in the rod experience an attractive force and move closer to the sphere, while an equal amount of positive charge is left at the other end of the rod. Thus, the rod becomes polarized. If the positively charged end of the rod is now grounded, the positive charge is able to flow to ground. If the ground wiring is removed and the charged sphere is moved to a distance, the rod is left negatively charged by induction [13].

Induction charging is essential in charging of conductors for instance in the electronics industry. The phenomenon is important in charging of insulators as well since image charges are induced on metal surfaces when a charged insulator is nearby. The resulting attractive force may cause particles to adhere in the surface.

2.9 Charge decay

In many situations, it is important to evaluate the time that is required for the accumulated charge to decay to ground [82–85]. If the rate of charge decay is lower than the rate of charge accumulation, the charge accumulates on the material. The decay rate depends on the capacitance on which the charge is stored, on the resistivity of the material, and on the remaining charge. The decay is fastest when the remaining charge is the highest and is exponentially reduced as the amount of charge is reduced. For materials that obey Ohm's law, this is mathematically expressed as

$$Q(t) = Q_0 \exp\left(-\frac{t}{\epsilon_r \epsilon_0 \rho}\right), \tag{2.5}$$

where $Q(t)$ is charge at time t, Q_0 is initial charge, ρ and ϵ_r are resistivity and relative permittivity of the material, and ϵ_0 is vacuum permittivity. The product $\tau = \epsilon_r \epsilon_0 \rho$ is known as the time constant. It describes the time that is required for the charge to

decay to $1/e$ of the initial value [13]. However, studies have shown that the decay is not strictly exponential in general [86]. Ohm's law is valid only for a homogeneous conductor whose conductivity is constant. Therefore, insulators do not satisfy Ohm's law, and eq. (2.5) is not strictly valid for insulators. Seaver [87, 88] has derived a general equation for the charge decay:

$$\rho_p(t) = \frac{\rho_{p0} \exp(-t/\tau_m)}{1 + \frac{\tau_m}{\tau_p}\left[1 - \exp(-t/\tau_m)\right]}, \tag{2.6}$$

where $\rho_p(t)$ is the charge density at time t, ρ_{p0} is the initial charge density, τ_m is a material time constant, and τ_p is a time constant related to the excessive charge. The equation is independent of the type of the material (solid, liquid, gas) or its nature (conductor, insulator).

The resistivity of a material can be used, at least to some extent, to estimate the charge decay. In practice, it is often necessary to measure the charge decay directly by monitoring the decay of the electric field or voltage as a function time rather than rely solely on resistivity measurements.

In industry, it may be necessary to ground conductive parts in order to increase the rate of charge decay so that dangerous discharges would not occur [89, 90]. For example in electrostatic protected areas, the floors are made of dissipative materials. This allows the accumulated charge to dissipate safely from the personnel to ground.

2.10 Electrostatic discharge

When the amount of accumulated charge in a material increases, the resulting electric field may eventually reach a limiting value for discharging. In air under normal conditions, the value is 3 MV/m and is known the dielectric strength of air. Therefore, the maximum net charge on a surface is limited to $2.7 \cdot 10^{-5}\ \mathrm{C/m^2}$. If this limit is reached, an electrostatic discharge (ESD) may occur. In a discharge, all or a part of the energy that is stored in the accumulated charge is released through a hot discharge channel. The type of discharge depends on the types of materials involved (conductors or insulators) and the geometry of the system [91].

According to the "charge relaxation model" by Matsuyama and Yamamoto [92, 93], the discharge plays an important role in the contact charging. When the contacting objects are being separated, a gaseous discharge may occur due to an increased electric field between the surfaces, and a part of the charge that was transferred in the contact is able to relax. The residual charge is observed on the surfaces after the separation. The

Paschen's law [94] is used to estimate the breakdown voltage between the objects [95, 96].

One of the most dangerous consequence of static electricity is a dust explosion [97]. The discharge may ignite the surrounding dust cloud of fine particles. The situation becomes more dangerous if flammable gases are also present in the surrounding atmosphere [91]. The explosions are usually characterized by the minimum ignition energy (MIE), which is the minimum energy that is required for a flammable atmosphere to ignite.

Lightings are examples of electrostatic discharges in nature. ESD problems are a major inconvenience in the electronics industry [98]. As modern electronic components are becoming smaller and more compact, they become more sensitive to the discharges [99].

2.11 Effect of material and environmental properties on charging

2.11.1 Nature of the contact

The nature of the contact between the contacting bodies has a significant effect on the charging. It is well known that rubbing increases the amount of transferred charge, but the reason for this is not completely understood. A common explanation is that the charging is enhanced due to an increase in the local temperature [13]. The applied force between the bodies, the contact surface area, the contact time, and the number of contacts are among the most crucial parameters that affect charging. In some contact studies, mercury has been used as the contacting metal in order to control the contact area. The contact with mercury is frictionless since it is liquid at room temperature. In addition, mercury is a metal and thus its electronic properties can be described with the concept of metal work function. Its work function can even be modified by alloying [100, 101].

Based on studies by Haenen [83], the generated charge in a polymer–metal contact depends on the applied force F as $Q \propto F^{\alpha}$ where the exponent α lies between 1/3 and 1. Relating the generated charge to the force is based on contact mechanical theories of deformation which give such a relationship for the true contact area and applied force [102]. Matsusaka et.al. [44] studied the charging of an elastic sphere in repeated contacts with a metal plate. They observed that the transferred charge was proportional to the maximum contact area in the impact. Moreover, the contact area increased when

the impact velocity was increased. Thus, the effect of force on the charging was related to an increase in the contact area.

Many experiments show an increase in the charging when the sliding velocity is increased. In some cases, a maximum or even the change in the sign of the charge has been observed. However, Lowell and Truscott [59] found no relationship between the charge and the velocity.

2.11.2 Surface roughness

Studies with glass samples of different degrees of surface roughness showed that the position of glass in the triboelectric series become more negative as the roughness was increased [103]. Angus and Greber [104, 105] observed that when glass samples with different degrees of roughness were rubbed together, the rougher sample became negatively charged and the smoother sample positively charged. They explained this with differences in the concentrations of excited electrons.

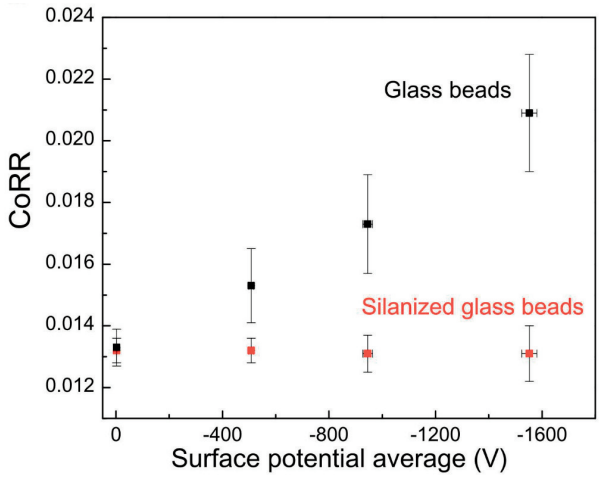

Figure 2.9: The generated surface potential on teflon sheets as a function of the coefficient of rolling resistance (CoRR) for untreated and silanized glass beads [106]. The figure is licensed under a Creative Commons Attribution-NonCommercial-NoDerivs 3.0 Unported License.

Surface roughness has a complex influence on the charge magnitude. Yao et.al. [107] studied charging of polypropylene and polyvinyl chloride objects with different degrees of surface roughness in a contact with a metal plate. They observed that the generated charge values first increased as the roughness was increased, but then decreased after

a critical point. Burgo et.al. [106] studied the charging of glass beads on teflon sheets with different friction coefficients. They observed that increase in the friction coefficient resulted in higher charging with untreated glass beads but had no effect on silanized glass beads (Fig. 2.9). Computer simulations by Yu et.al. [108] showed that the generated charges usually decreased with roughness but certain roughness levels resulted in higher charges compared to a smooth surface. Karner et.al. [109, 110] observed that and increased surface roughness increased charging for pure mannitol but had no effect when mannitol was mixed with the adhesive salbutamol sulphate, since mannitol particles became covered with salbutamol sulphate particles. Neagoe et.al. [111] concluded that in their charging experiments, surface roughness increased the contact points and therefore resulted in higher charge levels.

2.11.3 Relative humidity and temperature

A number of studies have shown that an increase in relative humidity usually decreases the measured charge values [112–124]. However, it is difficult to say if the transferred charge in the contact is actually smaller, if the backflow of the transferred charge during the separation is higher, or if the transferred charge can more quickly flow to ground. The effect of humidity is usually explained with a decrease in the surface resistivity as water molecules adsorb onto the material surface [112, 125–127]. However, it has also been observed that humidity increases charging [128], and in some studies the charging first increased and then decreased [129, 130]. Usually increasing the humidity is a simple way of reducing charging in industry. However, most materials need a relative humidity of over 70 RH% for this to be effective. A level of humidity this high is often impractical, *e.g* in powder processing units [131].

Greason [43] observed that an increase in temperature had a decreasing effect on the charging values due to a decreased resistivity. Perrin [132] observed that the volume resistivity of sugar powder decreased exponentially as the humidity or temperature was increased. Seaver [127] argued that a surface resistivity measurement of an uncoated insulator is nothing more than a measure of the adsorbed water on the insulator surface, suggesting that the water molecules form conductive chains under a high electric field during the resistivity measurement.

3. Measurements and instrumentation

3.1 Characterization of electrostatic charge

3.1.1 Faraday cup

When the electrostatic charge of a powder is of interest, one of the most commonly used instruments is the Faraday cup (or the Faraday pail). The Faraday cup consists of two conductive cups, one inside the other, that are insulated from each other. The outer cup is grounded and it acts as a shield against external electric fields. When a charged object is placed into the inner cup, a charge of the same magnitude but of opposite polarity is induced into the cup [13]. As a result, a potential difference is induced between the cups. The induced voltage V is directly proportional to the charge Q of the object as $Q = CV$ where C is the capacitance of the Faraday cup and the measuring electronics. The capacitance can be calculated or measured. Usually the voltage is measured with an electrometer. Often the electrometer is used in a charge measurement mode: the charge is measured by integrating the input current. In this case, the capacitance of the cup does not need to be known. The charge-to-mass ratio or the specific charge Q/m of the sample can be obtained by weighing the sample after the charge measurement. In practice, the resistance between the inner and outer cup and the impedance of the electrometer should be as high as possible so that the charge does not decay to ground [13]. A schematic illustration of the Faraday cup is presented in Fig 3.1.

Special Faraday pails for different purposes have also been developed. One of the major sources of error in Faraday cup measurements include sampling charging as the sample is placed into the cup. To overcome this, the Faraday cup may be open-ended so that the object of interest flows through the cup [133]. This way, the measurement

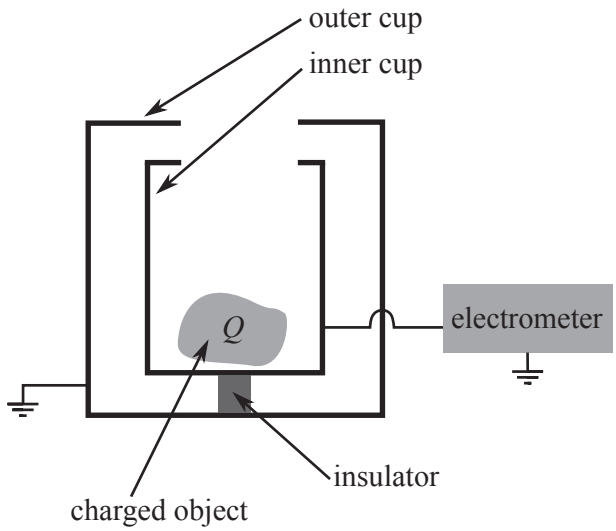

Figure 3.1: Schematic illustration of Faraday cup.

does not disturb the movement for instance of a powder flow but it must be ensured that all of the electric field lines originating from the charged object couple with the inner cup at some point. A filter may be installed into a Faraday cup to collect fine particles from air [134–137]. The measurement method may even be the opposite: in an inverse Faraday pail, the charged sample is placed into the inner cup and then sucked out or otherwise removed [65].

A Faraday cup measures only the net or overall charge of the sample. A set of Faraday cups can be used to study charge distribution in a powder sample if oppositely charged particles are first separated. The powder flow may be first directed into an electrostatic separator composed of two electrodes with high potential difference. The electric field between the electrodes deflects the particle trajectories: positively charged particles are drifted towards the negative electrode and vice versa. Thus, Faraday cups placed close to the electrodes collect particles of one polarity while a cup in the middle collects neutral particles [72].

3.1.2 Induction probes

The Faraday cup in its basic form is not suitable for on-line monitoring of charges for example on conveying belts or in pneumatic transportation lines. Sampling methods may be suitable for laboratory experiments, but on-line monitoring is preferential on an industrial scale so that preventive actions can be taken before the charge level becomes

too high.

In cases where the charge on large sheets or conveying belts is of interest, usually the electric field or voltage caused by the charge distribution is measured. The simplest type of field meter is the induction field meter. It consists of a metal sensor plate which becomes charged by induction in the presence of an external electric field. The most widely used electric field meter is the rotating-vane field meter where a grounded butterfly-rotor rotates in front of the sensor plate. At turns, the sensor plate is exposed to the electric field and shielded from it. The amplitude of the alternating voltage is proportional to the electric field [13]. However, electric field meters should generally be used to study rather large surface areas and from large distances since their spatial resolution is rather poor [138]. Non-contact electrostatic voltmeters are better for smaller surfaces. In non-contact electrostatic voltmeters, the voltage of the surface is measured instead of the resulting electric field. The feedback circuitry increases the potential of the voltmeter sensor until it matches the voltage of the surface. The measured value is independent of the distance between the sensor and the surface within a certain specified range [138].

In on-line charge measurements of powder in fluidized beds or pneumatic transport, induction probes are often used. The powder particles either impact the probe or pass it. If the particle is charged, a charge of the opposite polarity is induced into the probe, and the resulting voltage or current signal can be measured. In the voltage mode, the impedance of the probe is kept as high as possible, whereas in the current mode, the probe is grounded.

If the charged particle passes the probe without contact, the probe voltage increases to its maximum value and then returns back to its initial value. The current signal is bipolar: it increases as the particle approaches but then flips to the other polarity after the passing, finally decaying to zero. The areas of the positive and negative peaks are the same. The peak value of the voltage signal and integrated current signal are proportional to the charge of the particle.

If the charged particle hits the probe and sticks to it, the probe voltage first rises as the particle approaches, then reaches its maximum value upon the impact and stays at this value. The current signal, on the other hand, increases during the approach but decreases rapidly to zero when the particle sticks to the probe surface. The change in voltage and the area of the current signal are proportional to the charge of the particle.

If the charged particle, on the other hand, makes impact with the probe but does not stick to it, the voltage after the contact is different to the initial voltage since charge

transfer takes place between the particle and the probe. The current signal first reaches its maximum during the approach but flips to the opposite polarity and decays to zero as the particle goes further. However, the areas of the positive and negative peaks are not the same due to the charge transfer.

In practice, the recorded signals are often hard to analyse due to the chaotic nature of powder dynamics *e.g.* in a powder flow or fluidization. In fluidized beds, a large variety of methods has been proposed over the years. Recently, He et.al. [139, 140] presented a dual-tip probe consisting of two different materials (Ni and TiN) for on-line measurements in particle flow and in bubbling two-dimensional fluidized beds. Particles hitting the probe tips will transfer charge with the tips. The charge transfer depends on the initial charges, impact velocity and also on the work functions. Using different tip materials, different charge transfers were observed. Analysis on the recorded current signals combined with previously determined empirical equations resulted in good results when compared to Faraday cup experiments. Other measurement methods in fluidized beds have been recently reviewed by Mehrani, Murtomaa and Lacks [141].

3.2 Measuring electrical resistivity

Electrical resistivity is a fundamental surface and volume property of a material that describes its ability to resist the flow of an electrical current. Therefore, it greatly affects the charge decay rate. Volume resistivity ρ can be measured for example by placing the sample between two parallel electrodes. A voltage V is applied across the electrodes and the resulting electric current I is measured. When the surface area A of the electrodes and their separation distance d are known, the resistivity can be determined from the equation

$$\rho = R\frac{A}{d} = \frac{V}{I}\frac{A}{d}, \tag{3.1}$$

where $R = V/I$ according to Ohm's law [13]. The parallel-plate method is suitable *e.g.* for powder resistivity measurements. The electrodes and the container where the powder is poured, are commonly known as a resistivity cell. In the resistivity cell described in the British Standard 5958 [142], the diameter of the electrodes is 50 mm, and their spacing is 5 mm.

For bulk solids, the parallel-plate method or any other two-terminal method may not be the optimum, since the contacts between the electrodes and the sample surface play an important role [13]. If the contact is poor, the contact resistance may significantly affect the measured resistivity value. In addition, the true contact area is hard to determine

accurately as the surfaces are not ideally smooth. To overcome the contact resistance problems, four-point measurements are often used. In the four-point measurement, four equally spaced point-electrodes are connected to the sample: a current I is supplied into the sample with the two outermost terminals, and the other two terminals are connected between these two to measure the voltage drop ΔV. The volume resistivity can be calculated from the equation

$$\rho = 2\pi d \frac{\Delta V}{I}, \tag{3.2}$$

if the sample is thick, or the from equation

$$\rho = \frac{\pi}{\ln 2} \frac{\Delta V}{I} t, \tag{3.3}$$

if the sample is thin. In the equations, d is the spacing between the terminals and t the sample thickness [86].

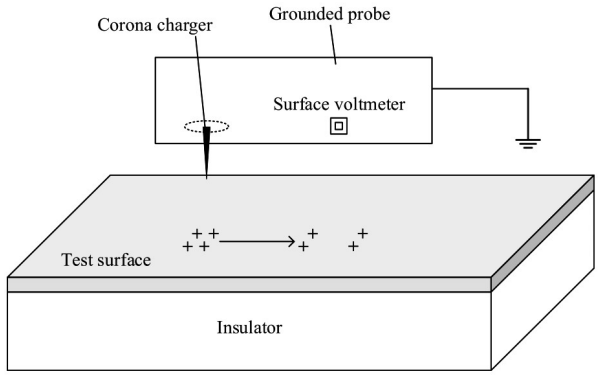

Figure 3.2: Basics of a non-contact surface resistivity measurement. Reprinted from [143] with permission from Elsevier.

There is a great variety of configurations available for measuring surface resistivity. With a simple two-pin method, the contact resistance is often too large for reliable results. The four-point method, described above, can also be used to determine the surface resistivity. In a commonly used method, two concentric electrodes are used: the inner electrode is disc-shaped and it is surrounded by a ring-shaped outer electrode. The other methods to improve the measurements include *e.g.*, painting parallel stripe electrodes onto the sample surface. In all these methods, a voltage is applied and the resulting current is measured. The equation to obtain the surface resistivity depends on the measurement geometry [144]. Recently, non-contact surface resistivity measurement methods have been proposed [143, 145]. In the non-contact methods, a part of the

studied surface is charged with a corona-charger. The rate at which the charge propagates on the surface is proportional to the surface resistivity and can be measured with a non-contact voltmeter (Fig. 3.2).

Both volume and surface resistivity measurements may suffer from poor reproducibility. For instance, particle packing and applied force have a significant influence on the powder resistivity [146–148]. The surface resistivity of surfaces with an awkward shape may be difficult, if not impossible, to measure.

4. Static electricity in some industrial processes

In industrial processes, static electricity is usually considered an undesirable phenomenon. Despite this, it has many valuable applications, such as electrostatic painting [149, 150], electrostatic powder coating in the food industry [151–156], electrophotographic printing or xerography [157–160], electrostatic precipitation [161–163], electrospraying [164–166], and electrospinning [167–169].

4.1 Particle and powder technology

In industrial processes where powders are handled, the powders become electrostatically charged due to numerous particle–particle and particle–surface contacts when the powders are, for instance, transferred or mixed [170].

High charge build-ups are often observed in the high-velocity pneumatic transport of powders especially if the powder is transferred through an insulating pipe or a conductive pipe with an insulating inner layer. However, charging occurs with conductive pipes as well. In pipe-flows, the charge is usually monitored with induction probes [139, 171, 172]. High charge levels can be generated also when powders are loaded into silos [173, 174], leading to a severe risk of an explosion, as discussed in section (2.10).

Electrostatic charging increases the adhesion/cohesion of the particles [153, 175–177]. For instance in the pharmaceutical industry, the packing behaviour, flowability, and manufacturing of powders, among other things, may be hampered as a result of an excessive electrostatic charge [178]. Pharmaceutical drug powders are usually mixed with an additive powder to improve, for instance, dosing accuracy. Highly charged small particles adhere easily to the surfaces of the transportation system, and the concentrations in the final drug–additive mixtures may considerably differ from the planned

concentrations. Another important example are dry-powder inhalers (DPIs), devices that are used to deliver the powdered drug into the lungs in aerosol form, for instance in the treatment of asthma. The micronized drug particles are mixed with larger carrier particles, such as lactose. Ideally, the drug particles will end up into the lower parts of the lungs while the carrier particles end up into the upper part of the respiratory tract. The drug particles may stick to the carrier particles if they become oppositely charged. If they do not separate as the operator inhales, the drug may never reach the lungs. On the other hand, a small electric charge enhances the deposition of the drug particles in the lungs [179]. The space charge of the aerosol particles has an important role in the upper region of the respiratory tract as the space charge tends to expand the aerosol cloud. The image charge acts in the lower parts on the alveolar region where the respiratory tract is very narrow and the particles are close to the walls of the tract. An image charge of the opposite sign is induced into the conductive wall, and the resulting electric field deposits the particle effectively [180–182].

4.2 Gas–solid fluidized beds

In fluidized beds, solid powder particles are under certain conditions transformed into a fluid-like state when an upward flowing gas counterbalances the gravitational force of the powder [183]. The fluidization is widely used in different industries, such as the chemical and pharmaceutical industry. For instance in the chemical industry, it is used for the catalytic reactions, and in the polyolefin industry it is used in the catalytic polymerization of ethylene to produce polyethylene. In pharmaceutical industry, it is used in granulation [184], coating [185, 186] and drying [187] processes. Due to the fluidization process, the powder particles are intensively mixed, resulting in a high heat transfer capability.

One of the biggest problems arises from the frequent particle–particle and particle–wall contacts [188]. The particles may become highly charged and adhere strongly onto the surface of the fluidization column [189]. Adhered particles may hamper the heat transfer between the powder and the column. The polymerization process, for instance, is exothermic. As a consequence, the particles may melt onto the surface and form ”sheets”, eventually resulting in the shut-down of the reactor [190]. The charging of the fluidized powder is affected by numerous parameters, such as powder and column materials, fluidization velocity, operating pressure and temperature, bubble size and rise velocity, particle size distribution, and so on [141, 190–192]. Bipolar charging

has been observed, usually so that the larger particles charge oppositely to the smaller particles [61, 63, 65]. Recently, Mehrani et.al. [141] and Fotovat et.al. [193] published comprehensive reviews about electrostatic charge build-up in gas–solid fluidized beds.

Numerous methods to measure the charge of the bed have been proposed over the years. As described in section (3.1.2) induction probes are often used in on-line measurements, *i.e.* during the fluidization process [188, 194, 195]. The signal (current or voltage) arises from contacts between the particles and the probe and also from variations in the charge density in the vicinity of the probe. An advantage of on-line methods is that it is not necessary to take a sample of powder since sampling may cause additional charging and may not be suitable for on-line monitoring in industry. In addition, induction probes can be installed in such a way that they do not hamper the fluidization process. However, a common problem with the method is that the measured signals are often hard to analyse. The measured signal depends not only on the charge of the object but also on the dynamics of the fluidized powder.

5. Aims of the study

The powder industry suffers from many undesirable effects and expensive consequences caused by triboelectric charging, a well-known yet poorly understood phenomenon. Therefore, electrostatics was considered worth studying in the Laboratory of Industrial Physics, University of Turku. The aim of the research was to study electrostatic phenomena from a practical point of view. The research, mainly experimental but also simulations, was done on subjects relevant to industrial processes, such as the transportation or fluidization of powders. Different measurement methods in various processes were developed. The triboelectric charging and electrical resistivity of powders and their mixtures were also studied. The effect of adhesion, humidity, and materials on charging were examined.

The resistivities of powders were studied as a function of mixture concentration and humidity, and better methods for studying the influence of humidity on resistivity were developed. In practice, it would be beneficial to be able to estimate the charging behaviour of powders based on measured resistivities because the measurement of resistivity is considerably easier than the measurements of charging for anyone who is not an expert in the field. Moreover, powder mixtures often charge in a more complex and unpredictable manner than single component powders. In the study, the charging and adhesion behaviour of lactose–salbutamol sulphate mixtures were examined at different humidities. These powders are used in the pharmaceutical industry, and excess charging have caused problems in the manufacturing process. Mannitol–dicalcium phosphate mixtures were studied during surface adhesion. Electrification usually increases the adhesion of fine particles to surfaces, and the charging behaviour may change due to the contamination. The main objectives were: 1) How to measure the electrostatic charging of a powder in contact with a clean surface, i.e. how can the effect of adhesion be evaluated? 2) At the point when particles start to adhere to the surface, how does the charging change? 3) How does the charging of a powder mixture change with adhesion?

The charging of powders in fluidized bed reactors can cause severe problems for

instance in the production of polyethylene and polypropylene. Therefore, an instrument for measuring the charging of fluidized powders was developed. The aim was to design a probe that could be used on-line during the fluidization process so that preventive actions could be taken before the charge level of the powder becomes too high.

6. Materials and methods

6.1 Electrometer

The most important instrument in the studies was the electrometer. Keithley 6514, 6517A and 6517B electrometers were used throughout the research. These electrometers can be used to measure voltage, current, resistance and charge. In the charge measurement mode, a voltage difference across a known internal capacitance is actually measured, and the charge is calculated. Keithley models 6517A and 6517B were equipped with a built-in voltage source (up to $\pm$1000 V). This feature was used in the resistivity measurements in papers I and V.

6.2 Charging methods and charge measurements

The used charge measurements can be divided into two methods: the direct method with Faraday cups and the induction method.

In charge measurements in papers I–IV, the Faraday cup was connected with a coaxial cable to an electrometer operated in the charge measurement mode. In paper VI, a light-weight Faraday cup was placed on a balance and, in order not to disturb the weighing with cables, the potential of the inner cup was measured with a non-contacting voltage probe (Trek Model 400 P-S probe connected to a Trek Model 400 voltmeter). The capacitance of the light-weight Faraday cup was determined experimentally: 30 induction charged water droplets with a known positive charge of 0.17 nC each were dropped into the cup and the resulting voltage ($V = 138$ V) was measured, resulting in $C = 3.7 \cdot 10^{-11}$ pF. The charge of the powder inside the cup was calculated from the measured voltage values using the determined capacitance.

In paper I, the powders (lactoses Prismalac 40 and Capsulac 60, sugar, monoammonium phosphate (MAP), and NaCl) were charged with a miniature fluidized bed. The fluidization column was made of stainless steel and was grounded during the measure-

ments. The powders were fluidized for 5 minutes at various humidities. After that, the powder was dropped into a Faraday cup to obtain the net charge. The fluidization velocity depended on the sample.

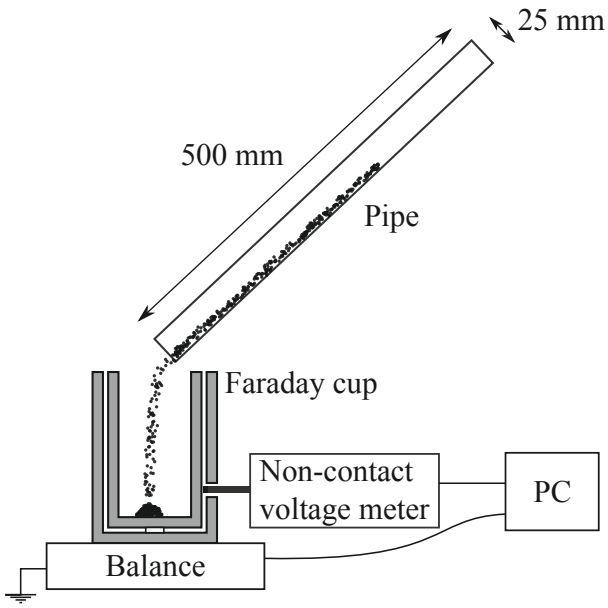

Figure 6.1: A schematic image of the measurement set-up used in Paper VI.

The sliding of powders in a pipe simulate to some extent the transportation of powders in industry but is less chaotic in nature [53]. Contact charging between the particles and the pipe as well as the effect adhesion can be studied [50, 56]. In papers IV and VI, the powders were charged by sliding in pipes of different materials. In paper IV, a small amount of powder (lactose, salbutamol sulphate, and their mixtures) was fed into the grounded stainless steel pipe. From the pipe, powder particles fell into the Faraday cup for the charge measurement. The sample was weighed before and after the sliding to study adhesion. In paper VI, stainless steel, polyvinyl chloride, polyethylene and polypropylene pipes were used to study the charging of mannitol, dicalcium phosphate and starch. The arrangement was similar to that in paper IV but the Faraday cup was placed on a balance. This enabled monitoring the cumulative mass and charge of the transferred powder simultaneously. The measurement set-up used in paper VI is presented in Fig. 6.1. Before the measurements in papers IV and VI, the pipes were carefully cleaned with tap water and ethanol. The powders were neutralized and placed on grounded metal plates to enable any excess charge to decay to ground.

In papers II and III, coaxial induction probes to be used in a fluidized bed were designed. In bubbling fluidized beds, the variations in the charge density are mainly caused by the rising bubbles in the charged powder [141]. Thus, a current signal can be measured as a bubble passes the probe. From the probes point-of-view, a signal induced by an air bubble moving charged fluidized powder is similar to a signal induced by a charged object moving in air. The working principle of the coaxial probes is presented in Fig. 6.2. The recorded bipolar current signals were integrated over time. In the next step, Gaussian curves were fitted to the integrated signal, and the amplitudes and the widths of the fitted curves were collected. Calibration equations were formed from these parameters and the amplitude ratios. In paper II, the probe was used in a miniature fluidized bed to measure the charge density of fluidized glass beads.

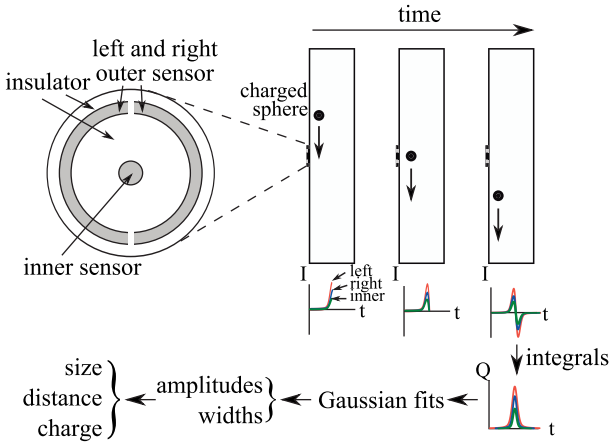

Figure 6.2: Schematic image and working principle of the developed coaxial probe.

The probes were first simulated with the COMSOL Multiphysics simulation software and then built and used in the measurements. The first version of the probe consisted of two coaxial sensors: a circular inner sensor (radius 1 mm) and a 1 mm thick ring-shaped outer sensor (outer radius 3 mm) which were both grounded. These sensors were separated with a 1 mm thick layer of an insulator. In the second version of the probe, the outer sensor was split vertically into half, so that bubbles passing the probe asymmetrically could be measured correctly, a major advantage compared to the first version. In addition, based on computer simulations, the diameter of the outer sensor was increased to improve probe sensitivity. The sensors were connected to amplifier electrical circuits for signal amplification and noise reduction. The signals were converted into digital form with an analog–digital converter NI USB-6008 (National

Instruments), and recorded using a LabVIEW 2009 coded programme.

6.3 Resistivity measurements

In papers I and V, powder resistivities were measured with three different resistivity cells. In the measurements, the powder sample was placed between two parallel electrodes, a voltage difference was applied across the electrodes, and the resulting current was measured. Resistivity was then calculated from equation (3.1). In all the measurements, the resistivity cell was surrounded by a metal chamber that enabled the control of the humidity of the surrounding air, and which also acted as a Faraday cage.

In paper I, a newly designed resistivity cell geometry and measurement method (Fig. 6.3 [196]) was compared to a standard resistivity cell described in the British Standard 5958 [142]. In the standard cell, the diameter of the circular electrodes was 50 mm and their spacing 5 mm. The amount of powder needed was roughly 0.5 dm^3. Traditionally, resistivity as a function of humidity is measured with a steady-state procedure where measurements are performed in multiple steps. The powder is humidified to a certain humidity, and the resistivity is measured when a steady-state humidity is reached. Next, the powder humidity is increased to another value and the procedure is repeated until the entire humidity range of interest is covered. These steady-state values are often regarded as the ”true” resistivity values. In the new one-step method, the resistivity was measured continuously as the humidity of the powder was changed from low to high or vice versa. As the humidity of the sample increased or decreased, a humidity gradient was created in the sample. From this reason, the current electrode connected to the electrometer was narrow and horizontal (5 mm $\times$ 30 mm), and surrounded by a grounded square-shaped guard electrode (50 mm $\times$ 50 mm). This ensured that the humidity in the volume between the electrodes was fairly constant. The guard electrode was insulated from the actual electrode, and its role was to ensure that the resulting electric field was homogeneous and that any current leaking into more conductive areas was not measured. The applied voltages were between 10 V and 1000 V, depending on the sample resistivities. Both steady-state and one-step measurements were performed.

In paper V, the used resistivity cell was small (40 mm $\times$ 40 mm $\times$ 36 mm) in order to reduce the amount of powder needed (Fig. 6.4). The electrode connected to the electrometer was fixed in place while the other one was movable and equipped with a spring so that the sample between the electrodes was compressed with a 10 N force. The width and height of the electrodes were 30 mm and 10 mm, respectively. The distance

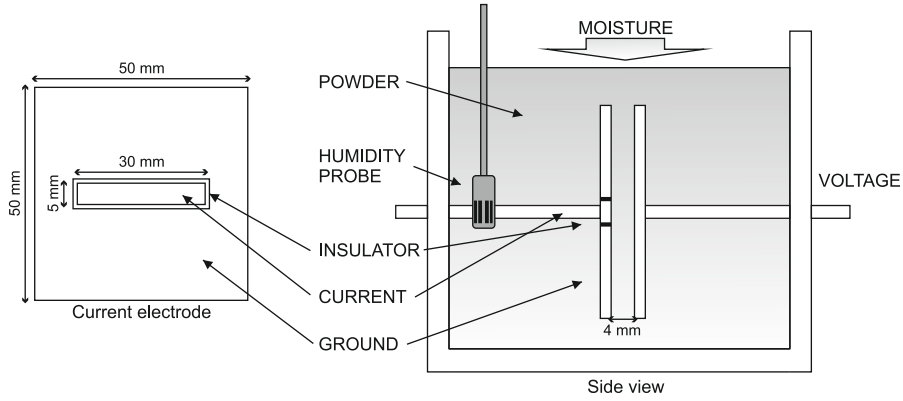

Figure 6.3: A schematic image of the resistivity cell used in paper I. Left: the cross section of the current electrode and the guard plate. Right: a side-view of the resistivity cell.

between the two electrodes (varied between 0.2 mm and 2.0 mm) was measured with a built-in scale. In order to prevent any leakage current flowing outside the region between the electrodes, a grounded copper guard ring was applied around the earthed electrode that was connected to the electrometer. The resistivities of powder mixtures with two components were measured as a function of mixture concentration and particle size. A voltage of 1000 V was used. In paper V, the measurements were performed in a dry atmosphere with a relative humidity of less than 5 RH%.

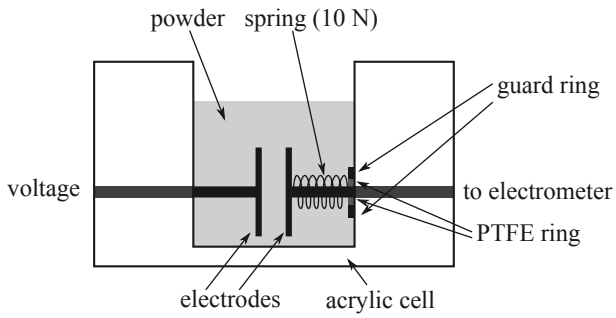

Figure 6.4: The resistivity cell used in paper V.

6.4 Other measurements

In paper IV, isothermal gas perfusion calorimetry (TAM 2277 Thermal Activity Monitor, Thermometric Ab, Sweden) measurements were performed to ensure that no chemical reactions took place in the samples despite the prolonged exposure to high relative humidity.

In paper V, particle sizes were measured as aerosols using laser diffraction (Helos H2370, Sympatec GmbH, Germany). In papers IV and VI, the particle sizes were estimated using a scanning electron microscope and an optical microscope, respectively.

In paper V, static relative permittivities of the bulk powder beds were measured. A sample of a powder was inserted between two circular parallel plate electrodes (radii 20.0 mm), and the capacitance C_x of the sample was measured with a multimeter (Fluke 289, Fluke Corporation, USA). The capacitance of the air-filled capacitor C_0 was determined with the same measurement set-up but without the powder sample while the distance between the electrodes was kept the same (1 mm). The relative permittivity ϵ_r was then calculated from the equation $\epsilon_r = C_x/C_0$.

In order to determine the volume fractions of the mixture samples in paper V, the true densities of the materials were measured with a pycnometer (AccuPyc 1330, Micromeritics Instrument Corp., USA). Tap densities were measured by inserting approximately 6 ml of powder into a tube with an inner diameter of 1.05 mm. The tube was then tapped against a bench until the height of the powder bed remained unchanged. The volume was calculated from the height of the bed and the mass was obtained when the sample was weighed.

6.5 Computer simulations

In papers II and III, the developed coaxial probes were simulated using the finite element method (FEM) with the COMSOL Multiphysics 4.3b software. In the analysis, a charged sphere was set to pass the probe inside a metal column, with different distances from the probe. The electric field $\mathbf{E}$ at the probe tip was calculated using equations

$$\nabla \cdot (\epsilon_0 \epsilon_r)\mathbf{E} = \rho \tag{6.1}$$

and

$$\mathbf{E} = -\nabla V, \tag{6.2}$$

where ρ is charge density, ϵ_0 is vacuum permittivity, ϵ_r is relative permittivity, and V is potential. The induced charge on the sensors was determined by first calculating the

surface charge density σ from equation

$$\mathbf{E} = \frac{\sigma}{\epsilon_0 \epsilon_r} \hat{u}_n \tag{6.3}$$

where $\hat{u}_n$ is the unit normal vector. The surface charge density σ was then integrated over the surface of the sensors.

7. Results and discussion on the papers

7.1 Paper I

Paper I is closely related to a previous paper by Murtomaa et.al. [196] where a novel one-step method for measuring powder resistivity as a function of humidity was introduced (Fig 6.3). In paper I, more one-step and steady-state measurements were performed with five different powders with a wide range of resistivities: two different lactose powders (Prismalac 40 and Capsulac 60), NaCl, monoammonium phosphate (MAP), and sugar.

Significant hysteresis was observed in the measured resistivity during the humidification and drying cycles. As the humidification began, water molecules adsorbed onto the powder particles, and started to diffuse deeper into the powder bed. The diffused water decreased the resistivity rapidly. As the once humidified powder was dried, the resistivity increased rapidly. The drying cycle eventually reached the point where the humidification had previously began.

With all of the samples, the resistivity decreased as the humidity was increased. The steady-state values draw relatively straight lines as a function of humidity on a semi-logarithmic scale. The end points of the hysteresis loops obtained in one-step measurements were close to the steady-state values, which is understandable since the powder eventually reaches a steady state at the end points. The steady-state resistivities were quite close to the center of the hysteresis loop, especially at low humidities (Fig. 7.1). Based on the observations, it was decided to present the one-step resistivities as a geometric mean of the humidification and drying values (Fig 7.2). It was observed that the one-step method provided meaningful results despite the hysteresis. For instance, the resistivity of a lactose powder was measured in 24 hours with the one-step method but took four weeks with the steady-state method.

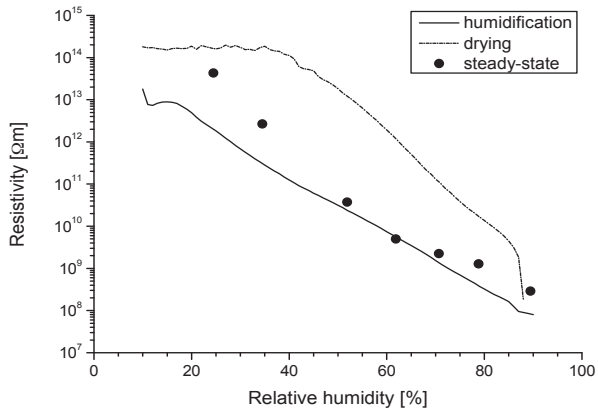

Figure 7.1: One-step measurement compared to steady-state resistivity measurements for Prismalac 40.

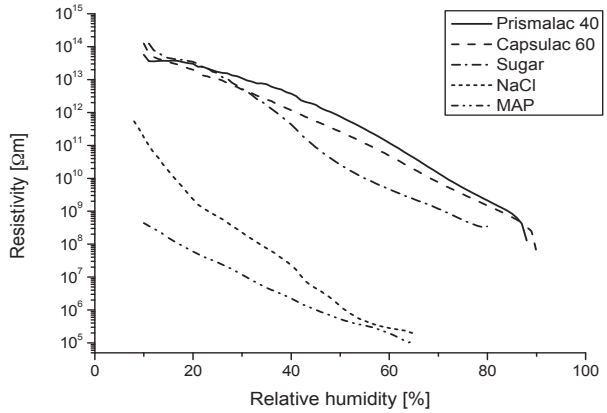

Figure 7.2: Calculated geometric mean values of the one-step resistivity measurements.

In addition to the resistivity measurements, the powders were charged by fluidizing in a miniaturized fluidized bed at different humidities. For the lactose powders, the increase in humidity clearly decreased the charging. NaCl and sugar did not acquire a notable charge. MAP showed a different behaviour: its charge increased slightly when the humidity was increased. By comparing the measured resistivities and charges it was noted that the charging was small for all of the samples when their resistivities were smaller than 10^{13} Ωm (Fig. 7.3). Charging decreased as the resistivity decreased, although MAP was again an exception.

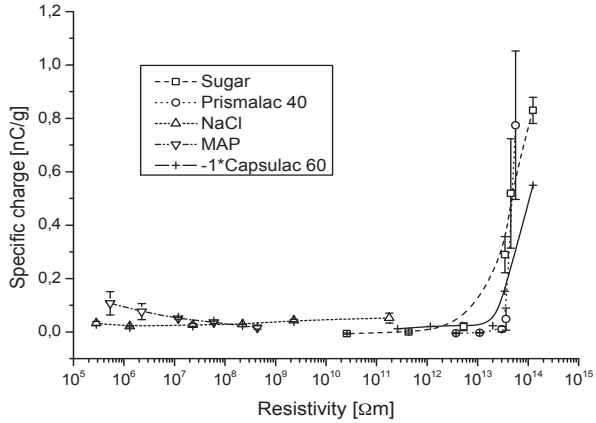

Figure 7.3: Specific charges for fluidized powders as a function of resistivity. Note that the absolute value of charge for Capsulac 60 is presented.

7.2 Paper II

In paper II, the aim was to develop an induction probe that could be used to measure the specific charge of fluidized powders in gas–solid fluidized beds on-line based on the signals caused by the deviation in the local charge density when a gas bubble passes the probe. The probe consisted of two coaxial sensors (a disc-shaped inner sensor surrounded by a ring-shaped outer sensor), and it was attached to the grounded fluidization column made of steel (Fig. 6.2). The probe and the column were separated from each other with an insulator.

The probe was first simulated with COMSOL Multiphysics. According to the simulations, the Gaussian curves fitted well to the induced charge data as the charged sphere passed the probe. The amplitudes and widths of the curves were larger for the outer sensor because its surface area was larger than that of the inner one. The amplitudes (A_o and A_i for the outer and inner sensors, respectively) and widths (W_o and W_i) were functions of the radius of the sphere and its passing distance. The amplitudes were also affected by the charge of the sphere, and the widths by the passing velocity. The amplitude ratio A_o/A_i and width ratio W_o/W_i did not depend on the charge or the velocity but were only functions of the radius and distance. Based on the simulations, it was concluded that the aforementioned parameters (charge, radius, distance, velocity) could be calculated from the shape of the signals.

The probe was experimentally calibrated with frictionally charged polypropylene spheres (radii from 2.0 mm to 12.0 mm). The spheres were set to pass the probe with

zero initial velocity, and the resulting current signals were measured. It was observed that the signals were relatively symmetrical. First, the current signals were integrated over time. Next, Gaussian curves were fitted to the integrated signals, and the calibration equations were determined from the amplitudes and the widths of the curves. In these measurements, the velocity could not be determined reliably since especially the width ratio W_o/W_i suffered from high scattering. The velocity needed to be fixed in order to calculate the other parameters.

After the calibrations, the probe was used in measurements. The charges of the passing spheres were reliably calculated (Fig. 7.4). Examples of calculated passing distance and radius are presented in Fig. 7.5. The probe was used to measure charging of glass beads in a miniature fluidized bed (inner diameter 35 mm, bed height 80 mm). It has to be pointed out that the spheres and bubbles had to pass the probe symmetrically, *i.e.* with no displacement from the probe axis. Single bubbles were injected into the glass beads with a bubble injector. The gas flow rate was kept just below the minimum fluidization velocity. After the fluidization, the powder was dropped into a Faraday cup, and the charge-to-mass ratio was determined. In the powder experiments, the measured signals were noisy but the calculated charge-to-mass ratios (between -0.07 nC/g and -0.27 nC/g) were close to the results measured with the Faraday cup (-0.11 nC/g).

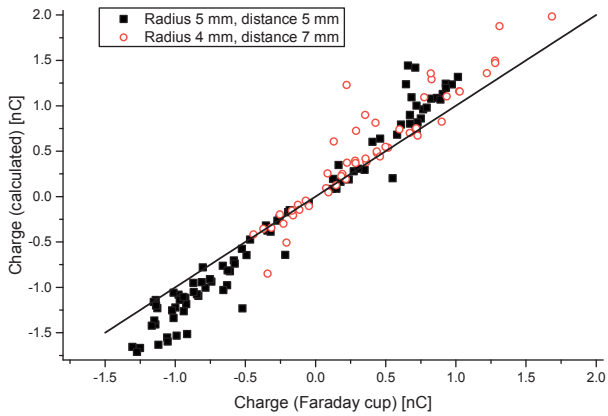

Figure 7.4: The calculated charge versus the measured charge with the first version of the probe. The solid line represents the line where the values are identical.

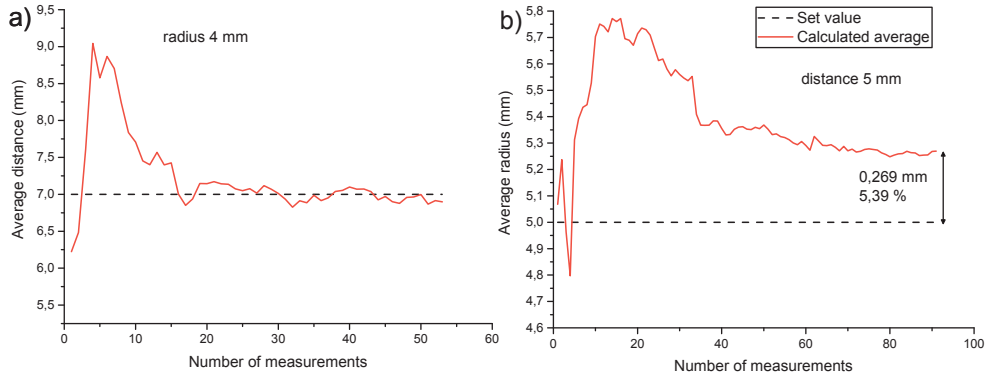

Figure 7.5: Running average of the calculated distance and b) calculated radius for repeated measurements with the first version of the probe.

7.3 Paper III

In paper III, the coaxial induction probe presented in paper II was further developed. In the improved version, the outer sensor was vertically divided into two adjacent sensors in order to measure the asymmetrically passing bubbles correctly. Asymmetrically passing objects were detected when the signal amplitudes from the left and right outer sensors were not equal.

In order to measure the charge-to-mass or charge-to-volume ratio of a fluidized powder, the radius of the passing bubble needs to be known with great accuracy since the volume is proportional to the cube of the radius. Simulations with COMSOL Multiphysics showed increasing the outer sensor radius would increase the probe sensitivity, enabling more accurate calculations and a wider detection range. From this reason, the radius of the outer sensor was increased. In addition, this probe version was designed to be used in a larger fluidized bed column (inner diameter 100 mm).

The probe was calibrated with charged polypropylene spheres (radii from 2.0 mm to 17.5 mm). Again, the calibration equations were determined from the amplitudes and widths of the integrated signals. As presented in Fig. 7.6, the charge of the spheres were reliably calculated.

The width ratio still suffered from high scattering and the velocity could not be calculated but had to be fixed. In fluidized beds, the bubble rise velocity is a function of the bubble size. Therefore, the velocity cannot be assumed to be constant. Bubbles of relatively same size could be inserted into the fluidized powder with a bubble injector in a laboratory scale, but this is not possibly in industrial scale fluidized bed reactors. The

development of the probe still continues in the laboratory.

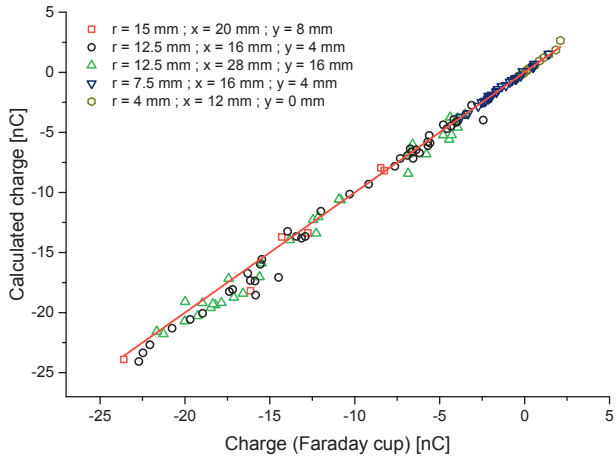

Figure 7.6: The calculated charge versus the measured charge with the second version of the probe. The solid line represents the line where the values are identical.

7.4 Paper IV

In paper IV, the study focused on charging measurements with pharmaceutical powders and powder mixtures. Lactose and salbutamol sulphate (SS) and mixtures containing 1 wt% and 2 wt% of SS in lactose were charged by sliding in a grounded metal pipe (length 500 mm, inner diameter 25 mm) with an angle of 50° relative to the horizontal level at different humidities in the range of 36 RH%–93 RH%. The powder was fed into the pipe using a grounded metal spatula. From the pipe, the particles fell directly into a Faraday cup for a charge measurement. By weighing the amount of the fed and the transferred powder, the adhesion of the powder particles was monitored and its effect on the charging was studied.

Lactose charged negatively and SS positively in contact with the metal pipe. An increase in the relative humidity clearly decreased the specific charge of lactose and both lactose–SS mixtures examined. The case was, however, not so obvious for pure SS, for which the humidity had no clear effect. On the other hand, SS was the only substance for which the charge values changed due to adhesion. For lactose and lactose–SS mixtures, the charge values remained constant throughout the measurements since the amount of adhered mass was only minor.

Humidity had a special kind of effect on the lactose–SS mixtures: the sign of the charge flipped from negative to positive as the humidity was increased and remained positive as the powders were again dried (Fig. 7.7). It is suggested that this was caused by changes in the mixture: when the humidity increased, the small SS particles stuck to larger lactose particles and remained adhered even if the powder was dried.

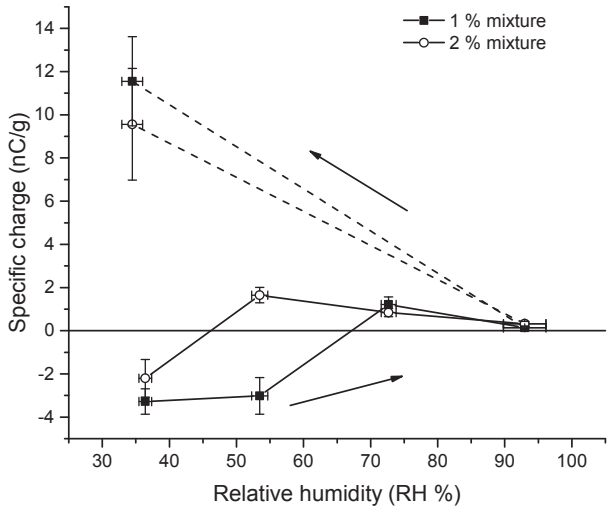

Figure 7.7: Average values of charges of lactose–SS mixtures as a function of relative humidity. The arrows represent the order in which the measurements were performed.

The adhesion behaviours of lactose and SS were clearly different: lactose hardly adhered onto the pipe surface whereas significant amounts of SS stuck to the pipe. The adhesion of the mixtures was also small. However, as the once humidified mixtures were slid at dry humidities, the adhesion increased but became less predictable. It was also observed that the already adhered powder had hardly any effect on the adhesion compared to a clean surface.

Young and Price [197] and Young et al. [198] also observed that the performance of lactose–SS dry powder inhalers declined significantly as the humidity was increased above 60 RH%. They also hypothesized that the increase in humidity increased the capillary forces between the SS and lactose particles, and as a consequence, the fine particle fraction of SS was reduced. However, they did not observe change in the sign of the charge with the mixtures.

7.5 Paper V

In paper V, the resistivity and relative permittivity of binary powder mixtures were studied and compared to theoretical models. Resistivities of powder mixtures have been studied surprisingly rarely, taking into account that powder mixtures often charge in a more complex and unpredictable manner than pure materials. Murtomaa and Laine [53] showed that the resistivity of a lactose—glucose mixture followed a linear relationship with a mass concentration. However, measurements were only performed using these two powders, and the resistivities of the pure materials were of the same order of magnitude. Thus, the linear behaviour could not be generalized for all powder mixtures.

For material mixtures, powders or bulks, the measured resistivity (known as the effective resistivity) depends significantly on the arrangement of the component materials between the electrodes. The Generalized Mixture Rule (GMR) [199–201] can be used to describe the physical properties of mixtures. If it is applied for the effective resistivity ρ_{eff}, the equation is

$$\frac{1}{\rho_{\text{eff}}^J} = \frac{\chi_1}{\rho_1^J} + \frac{\chi_2}{\rho_2^J}, \tag{7.1}$$

where ρ_1 and ρ_2 are the resistivities, and χ_1 and χ_2 the volume fractions (so that $\chi_1 + \chi_2 = 1$) of the phases 1 and 2, respectively. The exponent J can be considered as a scaling coefficient that depends on the shape and distribution of the mixture components. The cases $J = -1$ and $J = 1$ correspond to configurations where the phases are connected in series and in parallel, respectively. The case $J \to 0$ yields to a Random Model (RM). In the series configuration, the effective resistivity is dominated by the more resistive phase. This is the upper limit for the mixture resistivity. In the parallel configuration, the effective resistivity is dominated by the less resistive phase. The lower limit is given by the parallel configuration. In a random mixture, the phases have an equal impact on the effective resistivity.

For the effective relative permittivity ϵ_{eff}, the GMR equation is

$$\epsilon_{\text{eff}}^J = \chi_1 \epsilon_1^J + \chi_2 \epsilon_2^J, \tag{7.2}$$

where ϵ_1 and ϵ_2 are the relative permittivities of the phases 1 and 2, respectively. Cases $J = -1$ and $J = 1$ are equivalent to the series and parallel configurations, respectively, and $J \to 0$ yields to RM.

Four materials with a large range of resistivity were studied: sugar, potato starch, corn starch and NaCl. To study the effect of different particle sizes, three samples of NaCl were produced. A ”coarse” sample was produced by grounding by hand, and a

”fine” and a ”very fine” sample by using a ball mill pulverizer. Sugar was found to be the most resistive of the materials. Therefore, it was selected for mixing with the other powders. Binary mixtures containing 25 wt-%, 50 wt-% and 75 wt-% of sugar were produced. The volume fractions were calculated from the measured densities and the pre-determined mass fractions.

The measured effective resistivities are presented in Fig. 7.8. The figures include GMR curves (eq. (7.1)) that were fitted to the data. In addition, example curves with different J values were calculated using the resistivities of the pure materials. The J values were determined from the fitted curves. When sugar was mixed with corn starch, potato starch and very fine NaCl, the J value was close to zero, and therefore the results were in a good agreement with the values predicted by RM (Fig. 7.8a–c). In these mixtures, the particle sizes of the component materials were similar. However, when larger NaCl particles (coarse and fine NaCl) were present in the mixture, the effective resistivities were larger than those predicted by RM, and were closer to the series limit (J value close to -1) than to the random resistivity (Fig. 7.8d–e).

Since the behaviour for the mixtures that contained large NaCl particles was different compared to other mixtures, they were studied in more detail. With an optical microscope, it was observed that the finer, more numerous sugar particles coated the larger NaCl particles. It is speculated that the different particles became oppositely charged by triboelectrification when the mixtures were prepared causing the particles to stick. As a result, the mixtures were not randomly packed. Highly resistive small sugar particles isolated the more conducting NaCl particles from each other, and therefore there were no continuous paths of NaCl in the mixture. Thus, the effective resistivity was dominated by the sugar phase, and the structure of the mixtures were such that the effective resistivities were closer to the series configuration. When the particle sizes were similar, sugar did not coat the NaCl particles entirely, so that both NaCl and sugar formed continuous paths in the mixture. As a result, neither of the phases dominated and results predicted by RM were obtained.

The measured static relative permittivities are presented in Fig. 7.9 together with the GMR curves that were fitted using the previously determined J values. When sugar was mixed with corn starch, potato starch and very fine NaCl, the relative permittivity decreased according to RM (J close to 0) as the proportion of sugar was increased in the mixture. However, for a fine NaCl–sugar mixture, the permittivity values decreased more rapidly. Just like the effective resistivity, also the relative permittivity of NaCl–sugar mixtures with large NaCl particles showed a behaviour related to the series

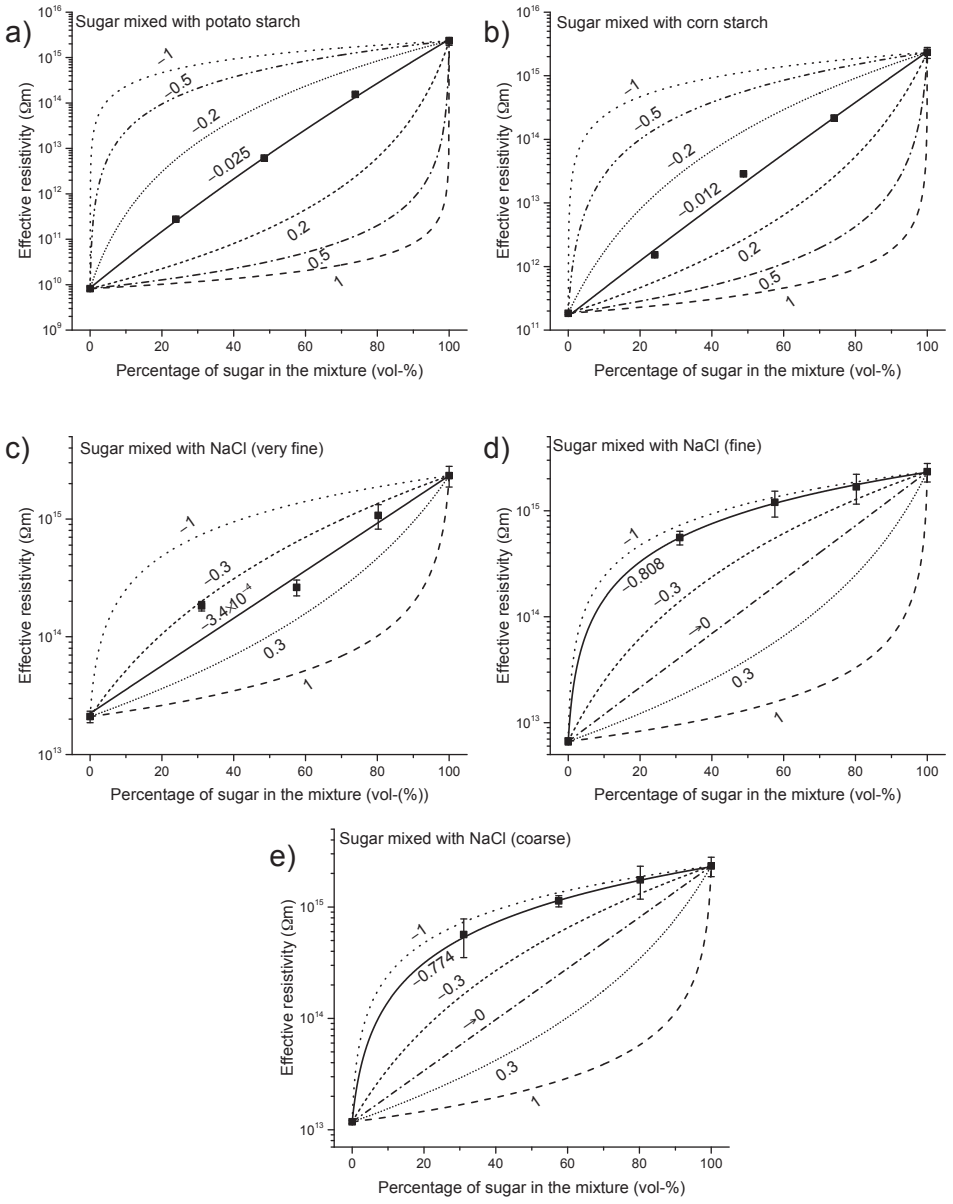

Figure 7.8: Measured and calculated effective resistivities as a function of the proportion of sugar in a) potato starch, b) corn starch, c)–e) NaCl with different particle sizes. The solid curve represents the GMR curve (eq. (7.1)) fitted to the measured data, while the dashed curves are calculated from the resistivities of the pure materials. The curves are labelled with the J value.

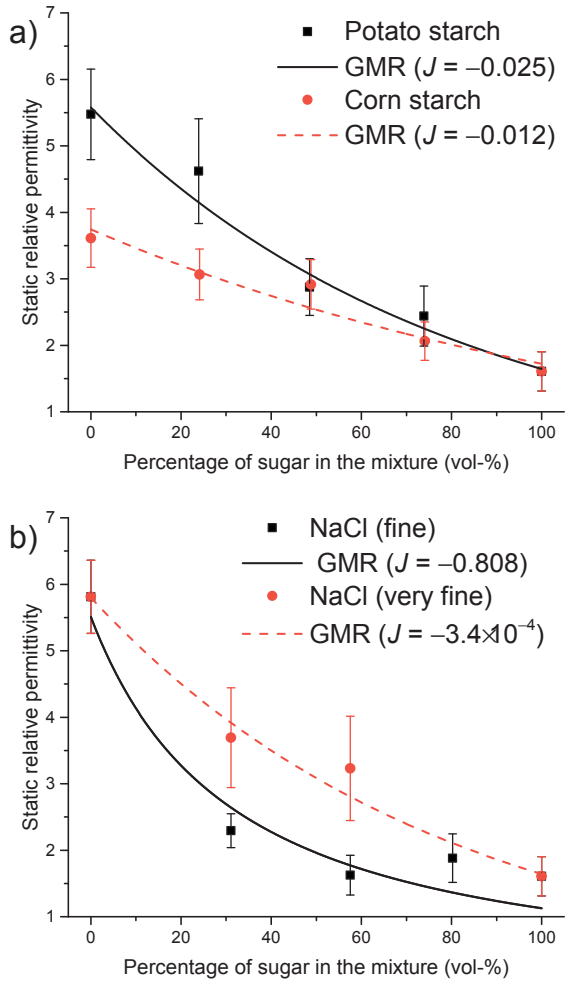

Figure 7.9: Measured static relative permittivities for sugar mixed with a) potato starch and corn starch, b) NaCl with different particle sizes. The presented curves were fitted to the data points with the previously determined J values.

configuration.

The obtained results can be used, for instance, to study how randomly powder mixtures are packed. Secondly, it can also be useful if a powder's resistivity is too high to be measured reliably in a traditional way: the powder could be mixed with some other material with a much lower resistivity. Measurements could be made for mixtures with different concentrations. Then, the resistivity of the powder in pure form could be obtained by fitting the best fitting curve described in the thesis and then by extrapolating

into a percentage value of 100 %. In addition, if the resistivities and particle sizes of the pure component materials are known, the volume fraction of a mixture could be calculated by measuring the resistivity of the mixture. For future research, the effect of particle size difference could be studied in more detail.

7.6 Paper VI

In paper VI, a method for measuring the effect of adhesion on the electrostatic charging of powders on-line was developed and used in the measurements. Like in paper IV, the powders were charged by sliding in a pipe. From the pipe, the particles fell into a light-weight Faraday cup that was placed on a scale. The cumulative charge and cumulative mass of the transferred powder were simultaneously measured. Mannitol, dicalcium phosphate and starch powders were charged with steel, polyethylene (PE), polypropylene (PP) and polyvinyl chloride (PVC) pipes. The determined triboelectric series is presented in Table 7.1.

Table 7.1: The determined triboelectric series

+	steel
	dicalcium phosphate
	mannitol
	PE
	starch
–	PP, PVC

According to a previous study by Murtomaa et.al. [56], the charge-to-mass ratio q of a fed powder batch decreases exponentially as a function of transferred mass m due to particle adhesion onto the pipe surface since contacts between particles of the same material lead to smaller charging compared to particle–pipe contacts. Mathematically this is expressed as

$$q(m) = q_1 e^{-m/m_0} + q_\infty, \tag{7.3}$$

where q_1 is amplitude, q_∞ is the saturation value, and m_0 is a characteristic mass describing the transferred mass at which the q is decreased to $1/e$ of its initial value. The smaller the m_0, the faster the saturation. In this study, however, the cumulative charge Q_c was measured instead of the charge-to-mass ratio. Q_c can be simply expressed as

the integral of the previous equation:

$$Q_{\mathrm{c}}(m) = \int q(m)\,\mathrm{d}m = -q_1 m_0 e^{-m/m_0} + q_\infty m + Q_0, \tag{7.4}$$

where Q_0 is an integration constant. The value $q_{m\to 0} = q_1 + q_\infty$ can be considered as the generated charge-to-mass ratio of the powder particles before adhesion, since it is the slope of the curve as cumulative mass approaches zero.

It was chosen to study the charging of mixtures containing mannitol and small amounts of dicalcium phosphate with a PP pipe since mannitol was located between PP and dicalcium phosphate in the triboelectric series, *i.e.* both of the powders gained a positive charge with the pipe but mannitol gained the opposite charge with dicalcium phosphate. The data is presented in Fig. 7.10. At first, the mixture curves followed the curve of pure mannitol, *i.e.* the contacts with the mannitol particles and the PP pipe surface dominated the charging. Next, the curves started to deviate from the mannitol curve. Eventually, the slopes changed to negative. This clearly indicates that the small dicalcium phosphate particles started to adhere to the surface of the pipe and that the particle–particle contacts between mannitol and adhered dicalcium phosphate started to dominate the charging process. With these three materials, negative charge was only expected for mannitol in contact with dicalcium phosphate. At certain concentrations, the saturation charge was close to zero.

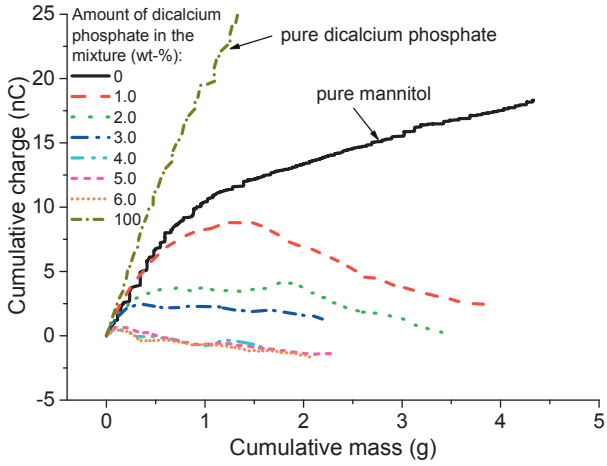

Figure 7.10: Cumulative charge as a function of the cumulative mass transferred for mannitol mixed with different concentrations of dicalcium phosphate in contact with PP pipe.

The equation (7.4) was fitted to the measured data for single component powders.

The equation was in very good agreement with the measured data, with R^2 values over 0.98 in all cases (Fig. 7.11). The fitted curves were differentiated in order to obtain the charge-to-mass ratio as a function of cumulative mass (eq. (7.3), Fig. 7.12).

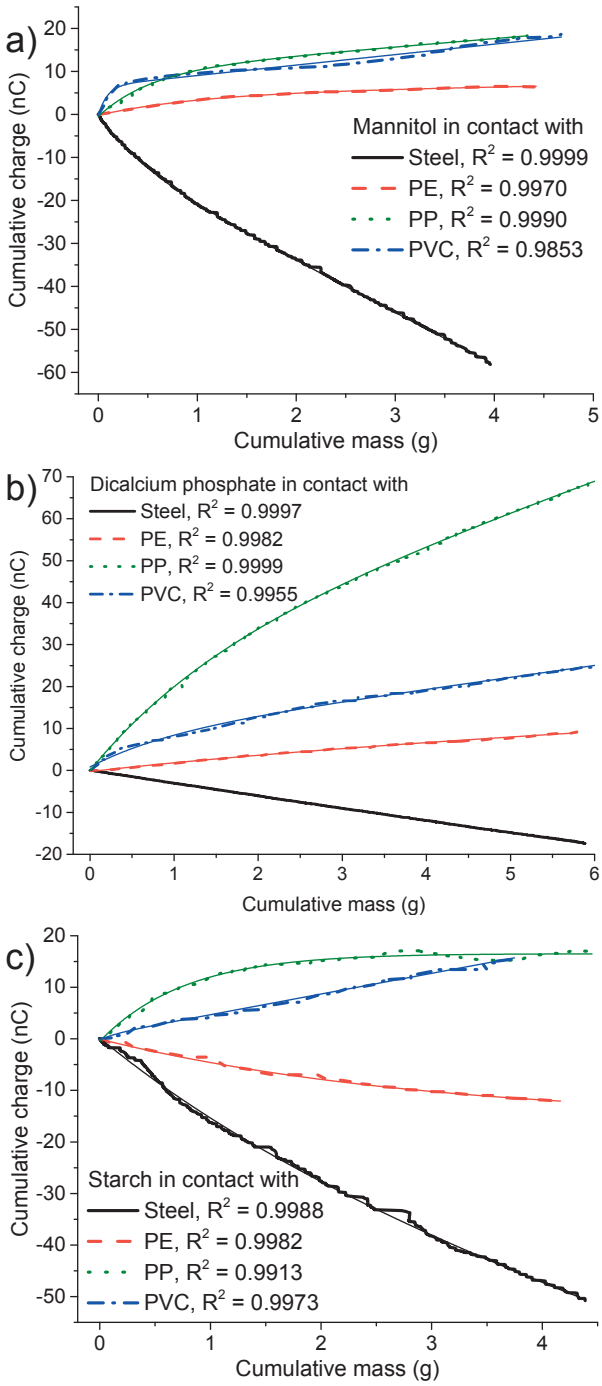

Figure 7.11: Cumulative charge as a function of the cumulative mass of the transferred powder for a) mannitol, b) dicalcium phosphate, c) starch in contact with different pipes. The fitted curves and the R^2 values are also presented.

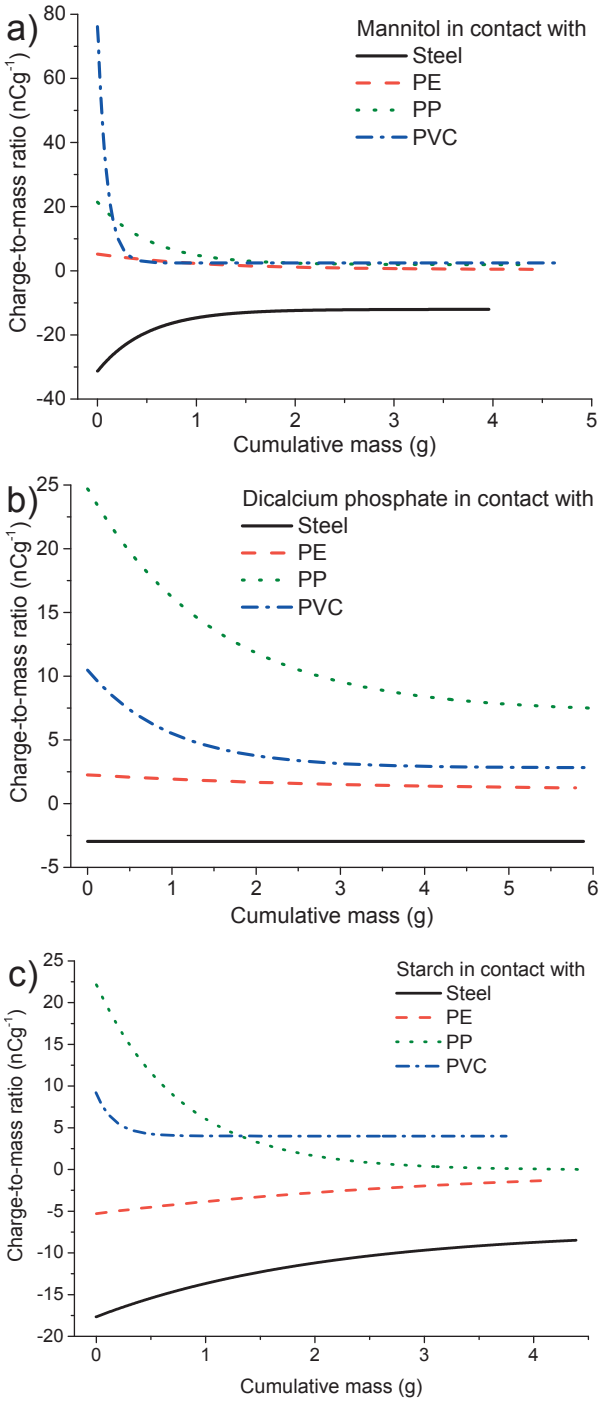

Figure 7.12: Defined charge-to-mass ratio as a function of the cumulative mass of the transferred powder for a) mannitol, b) dicalcium phosphate, c) starch in contact with different pipes.

8. Conclusions

The aim of this thesis was to develop measurement methods for various processes and to experimentally study the triboelectric charging and electrical resistivity of powders and powder mixtures.

A method for studying powder resistivity as a function of humidity was developed. It was observed that the resistivity decreased several orders of magnitude as humidity was increased. In addition, it was observed that the charging was the highest for powders with the highest resistivity. It was observed that the one-step method provided meaningful results despite the hysteresis. The one-step method proved to be significantly faster than the traditional steady-state measurements. For instance, the resistivity of a lactose powder was measured in 24 hours with the new one-step method but took four weeks with the traditional method.

Two induction probes for measuring the charge density of powder in a fluidized bed were developed. The probe was designed using computer simulations, calibrated with frictionally charged spheres, and finally tested in a laboratory-scale fluidized bed. However, the velocity of the passing bubble needed to be fixed. In order to be practical in the industrial scale fluidized beds, the method needs to be developed further.

The charging of lactose powder and salbutamol sulphate and their mixtures were studied by sliding at different humidities. It was observed that humidity decreased the charging of lactose but did not affect the charging of salbutamol sulphate. The increase in humidity had a special effect on the charging of mixtures containing 1 wt% and 2 wt% of salbutamol sulphate in lactose. At low humidities, the mixtures charged negatively. As the humidity was increased, the charge polarity flipped from negative to positive. When the once humidified samples were dried, the polarity did not flip back to negative but remained positive. In addition, the adhesion behaviour of the mixtures became less predictable after the humidification. It was suggested that the small salbutamol sulphate particles adhered to larger lactose particles due to increased capillary forces and remained adhered even if the powder was again dried.

The electrical resistivity and relative permittivity of binary powder mixtures were studied. It was observed that the particle size difference of the component materials played an important role in the effective resistivity and relative permittivity. The obtained results can be used, for instance, to study how randomly powder mixtures are packed. Secondly, it can also be useful if a powder's resistivity is too high to be measured reliably in a traditional way: the powder could be mixed with some other material with a much lower resistivity. Measurements could be made for mixtures with different concentrations. Then, the resistivity of the powder in pure form could be obtained by fitting the best fitting curve described in the thesis and then by extrapolating into a percentage value of 100 %.

A method for studying the charging of powders on-line during surface adhesion was developed and used in measurements. The powder was slid in pipes of different materials, and the charge and mass of the transferred powder were simultaneously monitored. The charge–mass curve decreased exponentially as the powder particles adhered to the surface of the pipe. The measurements matched the presented equations. The effect of adhesion on the charging was assessed by observing the slope of the measured curve at the very beginning of the measurement. In the studies with powder mixtures, the mixture components were chosen so that both of them gained charge of the same polarity with the chosen pipe. Furthermore, the main phase gained one polarity with the pipe and the other with the additive powder. For the mixtures, the powder with the higher concentration initially dominated the charging. The sign of the charge for the transferred powder changed as the additive powder started to adhere to the surface of the pipe, indicating that contacts between the two dissimilar powders started to govern the charging. With certain concentrations, the saturation net charge was close to zero.

Despite the long history of electrostatics, the theory behind triboelectric charging still remains poorly understood. In order to understand and control the phenomenon, more measurements have to be performed and instrumentation has to be improved in the future.

Bibliography

[1] D. J. Lacks and R. Mohan Sankaran, Journal of Physics D: Applied Physics **44**, 453001 (2011).

[2] K. Y. Law, I. W. Tarnawskyj, D. Salamida, and T. Debies, Chemistry of Materials **7**, 2090 (1995).

[3] M. D. Hogue, C. R. Buhler, C. I. Calle, T. Matsuyama, W. Luo, and E. E. Groop, Journal of Electrostatics **61**, 259 (2004).

[4] M. W. Williams, IEEE Transactions on Industry Applications **47**, 1093 (2011).

[5] M. W. Williams, Journal of Electrostatics **70**, 233 (2012).

[6] H. T. Baytekin, B. Baytekin, J. T. Incorvati, and B. A. Grzybowski, Angewandte Chemie - International Edition **51**, 4843 (2012).

[7] F. Galembeck, T. A. Burgo, L. B. Balestrin, R. F. Gouveia, C. A. Silva, and A. Galembeck, RSC Advances **4**, 64280 (2014), arXiv:_barata Materials and Techniques of polychrome wooden sculpture .

[8] G. S. Castle, Journal of Electrostatics **40-41**, 13 (1997).

[9] M. Murtomaa, *Electrostatic studies on pharmaceutical powders and aerosols* (Turun yliopiston julkaisuja AI 291, PhD thesis, 2002).

[10] C. K. Adams, *Nature's Electricity*, 1st ed. (Tab Books, Blue Ridge Summit, PA, 1987).

[11] D. J. Lacks, Angewandte Chemie - International Edition **51**, 6822 (2012).

[12] H. T. Baytekin, A. Z. Patashinski, M. Branicki, B. Baytekin, S. Soh, and B. A. Grzybowski, Science **333**, 308 (2011).

[13] J. A. Cross, *Electrostatics: Principles, problems and applications* (IOP Publishing Limited, Bristol, 1987).

[14] C. Kittel, *Introduction to Solid State Physics*, 4th ed. (John Wiley & Sons, Inc., New York, NY, 1971).

[15] F. C. Brown, *The Physics of Solids: Ionic Crystals, Lattice Vibrations, and Imperfections* (W. A. Benjamin, Inc., New York, NY, 1967).

[16] J. Lowell and A. Rose-Innes, Advances in Physics **29**, 947 (1980).

[17] S. Matsusaka, H. Maruyama, T. Matsuyama, and M. Ghadiri, Chemical Engineering Science **65**, 5781 (2010).

[18] W. R. Harper, Proceedings of the Royal Society of London Series **A 205**, 83 (1951).

[19] D. K. Davies, Journal of Scientific Instruments **44**, 521 (1967).

[20] D. K. Davies, Journal of Physics D: Applied Physics **2**, 307 (1969).

[21] R. G. Cunningham and H. P. Hood, Journal of Colloid And Interface Science **32**, 373 (1970).

[22] H. P. Hood and R. G. Cunningham, Journal of Colloid And Interface Science **32**, 444 (1970).

[23] A. G. Bailey, Journal of Electrostatics **51-52**, 82 (2001).

[24] D. Fenzel-Alexander, P. Brock, and A. Diaz, Langmuir **10**, 3323 (1994).

[25] L. S. McCarty, A. Winkleman, and G. M. Whitesides, Journal of the American Chemical Society **129**, 4075 (2007).

[26] L. S. McCarty and G. M. Whitesides, Angewandte Chemie - International Edition **47**, 2188 (2008).

[27] V. Lee, N. M. James, S. R. Waitukaitis, and H. M. Jaeger, Physical Review Materials **2**, 035602 (2018).

[28] W. R. Salaneck, A. Paton, and D. T. Clark, Journal of Applied Physics **47**, 144 (1976).

[29] J. Peart, KONA Powder and Particle Journal **19**, 34 (2001).

[30] I. I. Inculet, G. S. P. Castle, and G. Aartsen, Chemical Engineering Science **61**, 2249 (2006).

[31] J. Wong, P. C. L. Kwok, and H. K. Chan, Chemical Engineering Science **125**, 225 (2015).

[32] W. Kaialy, International Journal of Pharmaceutics **503**, 262 (2016).

[33] P. M. Ireland, Powder Technology **198**, 189 (2010).

[34] P. M. Ireland, Powder Technology **198**, 199 (2010).

[35] T. Matsuyama and H. Yamamoto, IEEE Transactions on Industry Applications **30**, 602 (1994).

[36] H. Watanabe, A. Samimi, Y. L. Ding, M. Ghadiri, T. Matsuyama, and K. G. Pitt, Particle & Particle Systems Characterization **23**, 133 (2006).

[37] H. Watanabe, M. Ghadiri, T. Matsuyama, Y. L. Ding, K. G. Pitt, H. Maruyama, S. Matsusaka, and H. Masuda, International Journal of Pharmaceutics **334**, 149 (2007).

[38] M. Sugihara, L. Dascalescu, G. Touchard, H. Romat, P. O. Grimaud, and S. Watanabe, Journal of Electrostatics **35**, 125 (1995).

[39] A. Ema, D. Yasuda, K. I. Tanoue, and H. Masuda, Powder Technology **135-136**, 2 (2003).

[40] B. C. O'Neill and T. R. Foord, Institute of Physics Conference Series **27**, 104 (1975).

[41] S. Cunningham and A. Goodings, Journal of Electrostatics **18**, 103 (1986).

[42] G. Touchard, A. Zerghouni, S. Watanabe, and J. Borzeix, Journal of Physics III France **1**, 1233 (1991).

[43] W. D. Greason, Journal of Electrostatics **49**, 245 (2000).

[44] S. Matsusaka, M. Ghadiri, and H. Masuda, Journal of Physics D: Applied Physics **33**, 2311 (2000).

[45] Y. Zhao, F. Zhou, J. Yao, and Z. Ji, Journal of Electrostatics **87**, 140 (2017).

[46] F. Chowdhury, A. Sowinski, M. Ray, A. Passalacqua, and P. Mehrani, Journal of Electrostatics **91**, 9 (2018).

[47] K. P. Homewood, J. Lowell, and R. M. Riley, Journal of Physics E: Scientific Instruments **18**, 846 (1985).

[48] S. Matsusaka and H. Masuda, Advanced Powder Technology **14**, 143 (2003).

[49] S. Matsusaka, M. Oki, and H. Masuda, Advanced Powder Technology **18**, 229 (2007).

[50] M. Murtomaa, K. Ojanen, and E. Laine, Journal of Electrostatics **54**, 311 (2002).

[51] M. Murtomaa, K. Ojanen, E. Laine, and J. Poutanen, European Journal of Pharmaceutical Sciences **17**, 195 (2002).

[52] G. Artana, G. Touchard, and M. F. Morin, Journal of Electrostatics **40-41**, 277 (1997).

[53] M. Murtomaa and E. Laine, Journal of Electrostatics **48**, 155 (2000).

[54] R. Gupta, D. Gidaspow, and D. T. Wasan, Powder Technology **75**, 79 (1993).

[55] D. K. Yanar and B. A. Kwetkus, Journal of Electrostatics **35**, 257 (1995).

[56] M. Murtomaa, P. Harjunen, V. Mellin, V. P. Lehto, and E. Laine, Journal of Electrostatics **56**, 103 (2002).

[57] M. M. Apodaca, P. J. Wesson, K. J. M. Bishop, M. A. Ratner, and B. A. Grzybowski, Angewandte Chemie - International Edition **49**, 946 (2010).

[58] P. E. Shaw and R. F. Hanstock, Proceedings of the Royal Society A **128**, 474 (1930).

[59] J. Lowell and W. S. Truscott, Journal of Physics D: Applied Physics **19**, 1273 (1986).

[60] J. Lowell and W. S. Truscott, Journal of Physics D: Applied Physics **19**, 1281 (1986).

[61] F. S. Ali, M. A. Ali, R. A. Ali, and I. I. Inculet, Journal of Electrostatics **45**, 139 (1998).

[62] S. Trigwell, N. Grable, C. Yurteri, R. Sharma, and M. Mazumder, IEEE Transactions on Industry Applications **39**, 79 (2003).

[63] H. Zhao, G. S. P. Castle, I. I. Inculet, and A. G. Bailey, IEEE Transactions on Industry Applications **39**, 612 (2003).

[64] W. M. Farrell, Journal of Geophysical Research **109**, E03004 (2004).

[65] P. Mehrani, H. T. Bi, and J. R. Grace, Journal of Electrostatics **63**, 165 (2005).

[66] K. M. Forward, D. J. Lacks, and R. M. Sankaran, Industrial and Engineering Chemistry Research **48**, 2309 (2009).

[67] K. M. Forward, D. J. Lacks, and R. M. Sankaran, Journal of Geophysical Research: Space Physics **114**, 3 (2009).

[68] S. R. Waitukaitis, V. Lee, J. M. Pierson, S. L. Forman, and H. M. Jaeger, Physical Review Letters **112**, 1 (2014), arXiv:1309.2578 .

[69] V. Lee, S. R. Waitukaitis, M. Z. Miskin, and H. M. Jaeger, Nature Physics **11**, 733 (2015).

[70] L. Zhang, X. Bi, and J. R. Grace, Procedia Engineering **102**, 295 (2015).

[71] D. J. Lacks and R. M. Sankaran, Particulate Science and Technology **34**, 55 (2016).

[72] J. R. Toth, A. K. Phillips, S. Rajupet, R. M. Sankaran, and D. J. Lacks, Industrial & Engineering Chemistry Research **56**, 9839 (2017).

[73] H. Yu, L. Mu, and L. Xie, Journal of Electrostatics **90**, 113 (2017).

[74] D. J. Lacks and A. Levandovsky, Journal of Electrostatics **65**, 107 (2007).

[75] D. J. Lacks, N. Duff, and S. K. Kumar, Physical Review Letters **100**, 1 (2008).

[76] K. M. Forward, D. J. Lacks, and R. M. Sankaran, Physical Review Letters **102**, 1 (2009).

[77] K. M. Forward, D. J. Lacks, and R. M. Sankaran, Geophysical Research Letters **36**, 1 (2009).

[78] K. M. Forward, D. J. Lacks, and R. Mohan Sankaran, Journal of Electrostatics **67**, 178 (2009).

[79] G. S. P. Castle and L. B. Schein, Journal of Electrostatics **36**, 165 (1995).

[80] R. Pham, R. C. Virnelson, R. M. Sankaran, and D. J. Lacks, Journal of Electrostatics **69**, 456 (2011).

[81] G. S. P. Castle, Proceedings of the 2008 ESA Annual Meeting on Electrostatics, Minneapolis, MN (2008).

[82] H. T. M. Haenen, Journal of Electrostatics **1**, 173 (1975).

[83] H. T. M. Haenen, Journal of Electrostatics **2**, 151 (1976).

[84] J. N. Chubb, Journal of Electrostatics **62**, 73 (2004).

[85] J. N. Chubb, Journal of Electrostatics **72**, 396 (2014).

[86] A. Blythe, Polymer Testing **4**, 195 (1984).

[87] A. E. Seaver, Proceedings of the ESA-IEJ Joint Meeting 2002, Northwestern University, Chicago, IL , 349 (2002), arXiv:0801.4182 .

[88] A. E. Seaver, Proceedings of the 2008 ESA Annual Meeting on Electrostatics, Minneapolis, MN (2008).

[89] E. S. Udoetok and A. N. Nguyen, Journal of Electrostatics **69**, 23 (2011).

[90] S. Egan, Journal of Electrostatics **88**, 183 (2017).

[91] M. Glor, Powder Technology **135-136**, 223 (2003).

[92] T. Matsuyama and H. Yamamoto, Journal of Physics D: Applied Physics **28**, 2418 (1995).

[93] T. Matsuyama and H. Yamamoto, Journal of Physics D: Applied Physics **30**, 2170 (1997).

[94] F. Paschen, Annalen der Physik **273**, 69 (1889).

[95] T. Matsuyama, M. Ogu, H. Yamamoto, J. C. Marijnissen, and B. Scarlett, Powder Technology **135-136**, 14 (2003).

[96] T. Matsusyama and H. Yamamoto, Chemical Engineering Science **61**, 2230 (2006).

[97] R. K. Eckhoff, *Dust Explosions in the Process Industries*, 3rd ed. (Gulf Professional Publishing, 2003) p. 487.

[98] S. Voldman, *ESD: Physics and Devices* (John Wiley & Sons, Inc., 2005).

[99] P. Tamminen, *Optimization of ESD Protection Methods in Electronics Assembly Based on Process and Product Specific Risks*, Ph.D. thesis, Tampere University of Technology. Publication; Vol. 1439 (2016).

[100] J. A. Medley, British Journal of Applied Physics **4**, 28 (1953).

[101] D. A. Hays, The Journal of Chemical Physics **61**, 1455 (1974).

[102] F. Nordhage and G. Bäckström, Journal of Electrostatics **3**, 371 (1977).

[103] G. Adams, *An Essay on Electricity* (Logographic Press, London, 1785).

[104] I. Greber and J. C. Angus, Proceedings of the 2016 Electrostatics Joint Conference, Purdue University, West Lafayette, IN (2016).

[105] J. C. Angus and I. Greber, Journal of Applied Physics **123** (2018), 10.1063/1.5024742.

[106] T. A. L. Burgo, C. A. Silva, L. B. S. Balestrin, and F. Galembeck, Scientific Reports **3**, 1 (2013).

[107] J. Yao, S. Cong, Y. Zhao, C. H. Wang, and Z. Ji, Advanced Powder Technology **28**, 2003 (2017).

[108] D. Yu, G. S. P. Castle, and K. Adamiak, Journal of Physics: Conference Series **142**, 012079 (2008).

[109] S. Karner, M. Maier, E. Littringer, and N. A. Urbanetz, Powder Technology **264**, 544 (2014).

[110] S. Karner, E. M. Littringer, and N. A. Urbanetz, Powder Technology **262**, 22 (2014).

[111] M. B. Neagoe, Y. E. Prawatya, T. Zeghloul, and L. Dascalescu, IOP Conference Series: Materials Science and Engineering **174** (2017), 10.1088/1757-899X/174/1/012003.

[112] J. W. Peterson, Journal of Applied Physics **25**, 501 (1954).

[113] S. Nieh and T. Nguyen, Journal of Electrostatics **21**, 99 (1988).

[114] D. T. Smith, Journal of Electrostatics **26**, 291 (1991).

[115] M. Grosvenor and J. Staniforth, Pharmaceutical Research **13**, 1725 (1996).

[116] J. Guardiola, V. Rojo, and G. Ramos, Journal of Electrostatics **37**, 1 (1996).

[117] T. Nomura, T. Satoh, and H. Masuda, Powder Technology **135-136**, 43 (2003).

[118] G. Rowley and L. Mackin, Powder Technology **135-136**, 50 (2003).

[119] A. Elajnaf, P. Carter, and G. Rowley, European Journal of Pharmaceutical Sciences **29**, 375 (2006).

[120] P. C. L. Kwok and H.-K. Chan, Pharmaceutical research **25**, 277 (2008).

[121] C. H. Park, J. K. Park, H. S. Jeon, and B. C. Chun, Journal of Electrostatics **66**, 578 (2008).

[122] S. K. Mohanta, B. Rout, R. K. Dwari, P. S. Reddy, and B. K. Mishra, Powder Technology **294**, 292 (2016).

[123] X. Shen, A. E. Wang, R. M. Sankaran, and D. J. Lacks, Journal of Electrostatics **82**, 11 (2016).

[124] K. Choi, M. Taghavivand, and L. Zhang, International Journal of Pharmaceutics **519**, 98 (2017).

[125] D. K. Das-Gupta and K. Doughty, Journal of Electrostatics **16**, 165 (1985).

[126] J. Paasi, S. Nurmi, R. Vuorinen, S. Strengell, and P. Maijala, Journal of Electrostatics **51-52**, 429 (2001).

[127] A. E. Seaver, Journal of Electrostatics **63**, 203 (2005).

[128] J. A. Wiles, M. Fialkowski, M. R. Radowski, G. M. Whitesides, and B. A. Grzybowski, The Journal of Physical Chemistry B **108**, 20296 (2004).

[129] S. Pence, V. J. Novotny, and A. F. Diaz, Langmuir **10**, 592 (1994).

[130] L. Xie, N. Bao, Y. Jiang, and J. Zhou, AIP Advances **6** (2016), 10.1063/1.4944831.

[131] *Electrostatics - Code of practice for the avoidance of hazards due to static electricity (CLC/TR 50404)* (European Committee for Electrotechnical Standardization, 2003).

[132] L. Perrin, A. Laurent, V. Falk, O. Dufaud, and M. Traoré, Journal of Loss Prevention in the Process Industries **20**, 207 (2007).

[133] H. Zhao, G. S. P. Castle, and I. I. Inculet, Journal of Electrostatics **55**, 261 (2002).

[134] M. Murtomaa, V. Mellin, P. Harjunen, T. Lankinen, E. Laine, and V. P. Lehto, International Journal of Pharmaceutics **282**, 107 (2004).

[135] M. Murtomaa, P. Pekkala, T. Kalliohaka, and J. Paasi, Journal of Electrostatics **63**, 571 (2005).

[136] A. Sowinski, L. Miller, and P. Mehrani, Chemical Engineering Science **65**, 2771 (2010).

[137] D. Song, F. Salama, J. Matta, and P. Mehrani, Powder Technology **290**, 21 (2016).

[138] M. A. Noras, Trek Application note **3002** (2002).

[139] C. He, X. T. Bi, and J. R. Grace, Powder Technology **253**, 1 (2014).

[140] C. He, X. T. Bi, and J. R. Grace, Particuology **21**, 20 (2015).

[141] P. Mehrani, M. Murtomaa, and D. J. Lacks, Journal of Electrostatics **87**, 64 (2017).

[142] "Code of Practice for Control of Undesirable Static Electricity, Part 1. General Considerations, British Standard 5958," (1991).

[143] K. Numayama, T. Sugimoto, and K. Taguchi, Journal of Electrostatics **98**, 17 (2019).

[144] J. Smallwood, Journal of Electrostatics **88**, 127 (2017).

[145] T. Sugimoto and K. Taguchi, Journal of Physics: Conference Series **646**, 012041 (2015).

[146] S. Marinković, C. Sužnejević, and M. Djordjević, Physica Status Solidi **743**, 743 (1971).

[147] M. Creyssels, E. Falcon, and B. Castaing, AIP Conference Proceedings **1145**, 123 (2009).

[148] J. M. Montes, F. G. Cuevas, and J. Cintas, Granular Matter **13**, 439 (2011).

[149] A. G. Bailey, Journal of Electrostatics **45**, 85 (1998).

[150] C. Schmitt and M. Lebienvenu, Journal of Materials Processing Technology **134**, 303 (2003).

[151] S. Elayedath and S. A. Barringer, Innovative Food Science and Emerging Technologies **3**, 385 (2002).

[152] A. E. Amefia, J. M. Abu-Ali, and S. A. Barringer, Innovative Food Science and Emerging Technologies **7**, 176 (2006).

[153] F. Halim and S. A. Barringer, Journal of Electrostatics **65**, 168 (2007).

[154] N. Sumonsiri and S. A. Barringer, Journal of Electrostatics **69**, 578 (2011).

[155] M. K. I. Khan, M. A. Schutyser, K. Schroën, and R. M. Boom, Journal of Food Engineering **111**, 1 (2012).

[156] T. Likitwattanasade and S. A. Barringer, Journal of Electrostatics **77**, 44 (2015).

[157] M. E. Scharfe and F. W. Schmidlin, Advances in Electronics and Electron Physics **38**, 83 (1975).

[158] R. W. Gundlach, Journal of Electrostatics **24**, 3 (1989).

[159] W. W. Carr, D. S. Sarma, F. L. Cook, S. Shi, L. Wang, and P. H. Pfromm, Journal of Electrostatics **43**, 249 (1998).

[160] C. B. Duke, J. Noolandi, and T. Thieret, Surface Science **500**, 1005 (2002).

[161] H. J. Lowe and D. H. Lucas, British Journal of Applied Physics **4**, S40 (1953).

[162] J. Zhu, X. Zhang, W. Chen, Y. Shi, and K. Yan, Journal of Electrostatics **68**, 174 (2010).

[163] Y. Xu, C. Zheng, Z. Liu, and K. Yan, Journal of Electrostatics **71**, 204 (2013).

[164] A. Jaworek and A. T. Sobczyk, Journal of Electrostatics **66**, 197 (2008).

[165] M. Nyström, M. Murtomaa, and J. Salonen, Journal of Electrostatics **68**, 42 (2010).

[166] J. Roine, M. Murtomaa, M. Myllys, and J. Salonen, Journal of Electrostatics **70**, 428 (2012).

[167] J. Doshi and D. Reneker, Journal of Electrostatics **35**, 151 (1995).

[168] H. Fong, I. Chun, and D. H. Reneker, Polymer **40**, 4585 (1999).

[169] M. M. Demir, I. Yilgor, E. Yilgor, and B. Erman, Polymer **43**, 3303 (2002).

[170] A. G. Bailey, Powder Technology **37**, 71 (1984).

[171] J. B. Gajewski, Journal of Electrostatics **37**, 261 (1996).

[172] J. B. Gajewski, Journal of Electrostatics **40-41**, 231 (1997).

[173] K. Choi, T. Mogami, T. Suzuki, and M. Yamaguma, Journal of Loss Prevention in the Process Industries **40**, 502 (2016).

[174] K. Choi, Y. Endo, and T. Suzuki, Powder Technology **331**, 68 (2018).

[175] D. A. Hays and J. C. Sheflin, Journal of Electrostatics **63**, 687 (2005).

[176] E. Šupuk, A. Zarrebini, J. P. Reddy, H. Hughes, M. M. Leane, M. J. Tobyn, P. Timmins, and M. Ghadiri, Powder Technology **217**, 427 (2012).

[177] H. Kweon, S. Yiacoumi, and C. Tsouris, Colloids and Surfaces A: Physicochemical and Engineering Aspects **481**, 583 (2015).

[178] J. N. Staniforth, in *Respiratory Drug Delivery IV*, edited by P. R. Byron, R. N. Dalby, and S. J. Farr (Interpharm Press, 1994) pp. 303–311.

[179] C. Melandri, G. Tarroni, V. Prodi, T. De Zaiacomo, M. Formignani, and C. C. Lombardi, Journal of Aerosol Science **14**, 657 (1983).

[180] W. Balachandran, C. N. Ahmad, and S. A. Barton, Institute of Physics Conference Series **No. 118**, 57 (1991).

[181] W. Balachandran, W. Machowski, E. Gaura, and C. Hudson, Journal of Electrostatics **40&41**, 579 (1997).

[182] A. G. Bailey, A. H. Hashish, and T. J. Williams, Journal of Electrostatics **44**, 3 (1998).

[183] D. Kunii and O. Levenspiel, *Fluidization Engineering*, 2nd ed. (Butterworth-Heinemann, 1991).

[184] D. F. de Andrade, E. G. de Oliveira, A. R. Pohlmann, S. S. Guterres, I. C. Külkamp-Guerreiro, and R. C. R. Beck, Powder Technology **326**, 25 (2018).

[185] A. Mehle, D. Kitak, G. Podrekar, B. Likar, and D. Tomaževič, International Journal of Pharmaceutics **546**, 78 (2018).

[186] R. Šibanc, M. Turk, and R. Dreu, Chemical Engineering Research and Design **134**, 15 (2018).

[187] M. Taghavivand, K. Choi, and L. Zhang, Powder Technology **316**, 171 (2017).

[188] D. Boland and D. Geldart, Powder Technology **5**, 289 (1972).

[189] J. Ciborowski and a. Wlodarski, Chemical Engineering Science **17**, 23 (1962).

[190] G. Hendrickson, Chemical Engineering Science **61**, 1041 (2006).

[191] Y. Tian and P. Mehrani, Journal of Electrostatics **76**, 138 (2015).

[192] F. Fotovat, K. Gill, J. R. Grace, and X. T. Bi, Chemical Engineering Science **167**, 120 (2017).

[193] F. Fotovat, X. T. Bi, and J. R. Grace, Chemical Engineering Science **173**, 303 (2017).

[194] A. Chen, H. Bi, and J. R. Grace, Journal of Electrostatics **58**, 91 (2003).

[195] M. Murtomaa, E. Räsänen, J. Rantanen, A. Bailey, E. Laine, J.-P. Mannermaa, and J. Yliruusi, Journal of Electrostatics **57**, 91 (2003).

[196] M. Murtomaa, E. Mäkilä, and J. Salonen, Journal of Electrostatics **71**, 159 (2013).

[197] P. M. Young and R. Price, European Journal of Pharmaceutical Sciences **22**, 235 (2004).

[198] P. M. Young, A. Sung, D. Traini, P. Kwok, H. Chiou, and H. K. Chan, Pharmaceutical Research **24**, 963 (2007).

[199] S. Ji, Q. Wang, B. Xia, and D. Marcotte, Journal of Structural Geology **26**, 1377 (2004).

[200] S. Ji, Journal of Geophysical Research B: Solid Earth **109**, 1 (2004).

[201] S. Ji, Q. Wang, B. Xia, and Z. Xu, Acta Petrologica Sinica **22**, 2067 (2006).

Annales Universitatis Turkuensis

UNIVERSITY OF TURKU

Grano Oy - Turku, Finland 2019

ISBN 978-951-29-7655-3 (PRINT)
ISBN 978-951-29-7656-0 (PDF)
ISSN 0082-7002 (Print)
ISSN 2343-3175 (Online)